RADIOMIC ANALYSIS OF SONOGRAMS FOR THE DETECTION OF TENDON DAMAGE

SAMUEL L. HUBERT

Thesis submitted to the Faculty of the
Virginia Polytechnic Institute and State University
in partial fulfillment of the requirements for the degree of

Master of Science

in

Biomedical Engineering

Vincent M. Wang, Chair
Albert J. Kozar
Miguel A. Perez

May 13, 2025
Blacksburg, Virginia
Keywords: Tendinopathy, Ultrasound, Texture, Biomechanics

RADIOMIC ANALYSIS OF SONOGRAMS FOR THE DETECTION OF TENDON DAMAGE

SAMUEL L. HUBERT

ABSTRACT

The exact precursors to tendinopathy can be multiple and nuanced. Further complicating effective diagnosis is the reliance on tendon pain as a measure of injury. Even severe tendinopathies can remain asymptomatic as overuse damage accumulates and diagnosis using quantitative indicators of damage is challenging. Hence, there is a critical need to establish biomarkers to assist in early detection of tendinopathy in at-risk populations such as athletes. One set of imaging biomarkers can be generated using radiomics. This technique extracts numerical values from medical images, such as those captured using ultrasound (US), for clinical decision-making. US images are the standard for confirming clinical tendinopathy diagnoses, as they are more accurate, less time-consuming, and less expensive than other modalities. Texture analysis, a subset of radiomics, uses algorithms to quantify the shade, alignment, and distribution of pixels within US images to assess the disease state of a tissue. Prior clinical studies of texture analysis have shown that it can reliably identify differences in tissue structure and composition. In symptomatic cases of tendinopathy, tendon US images appear darker and more disordered. One drawback to previous *in vivo* studies, however, is the large variation of higher order statistics between US images, likely due to changes in ultrasound transducer operation or patient positioning. To circumvent these limitations, imaging of an *ex vivo* tendon will be conducted simultaneously with loading in this study. A total of 14 juvenile, female porcine superficial digital flexor tendons were excised and loaded using an MTS Insight 10 load frame. US imaging was carried out using a Supersonic Imagine Aixplorer SLH20-6 transducer. After preloading at 2 N, each sample in the progressive strain group (n = 6) was subjected to progressively increasing strain levels (2, 4, 6, and 8%), utilizing a 25-minute stress relaxation at each strain magnitude with 20-minute recoveries. Once the stress stabilized, the equilibrium stiffness (E_{eq}) was calculated, and additional US images were taken. The onset of tendon damage was defined by a reduction in E_{eq}, as well as other mechanical parameters such as laxity and percent relaxation. The strain level at which this damage occurs informed extension parameters for the second group (n = 8), where US images were acquired before and after applying a single 10% strain ramp to induce damage. It was found that numerous parameters describing image texture correlated with reductions in tendon mechanical properties, with

novel data suggests that higher order parameters can serve as reliable imaging biomarkers of matrix damage and can be used in the future for clinical diagnostics.

RADIOMIC ANALYSIS OF SONOGRAMS FOR THE DETECTION OF TENDON DAMAGE

SAMUEL L. HUBERT

GENERAL AUDIENCE ABSTRACT

Tendinopathy is a type of degenerative tendon injury that develops from overuse. One major challenge is that many tendinopathies do not immediately cause pain, even when damage is severe, which makes it difficult to diagnose the condition before it becomes debilitating. To improve early detection, there is an urgent need to develop clinical methods that can reveal early signs of damage in the tendon. Currently, symptomatic tendinopathy is frequently confirmed by ultrasound (US) imaging, which uses sonic waves to visualize the tendon through the skin. One promising approach to streamlining this process is a method called radiomics, which converts medical images—like those acquired using US—to numerical data for analysis. This technique can look at patterns in these images, such as light and dark areas, to identify signs of tissue damage. Previous clinical studies have shown that radiomics can detect changes in tendon structure, but results can vary due to factors such as patient positioning during scanning. To avoid this pitfall, this study examined tendons dissected from pigs in a controlled lab setting. Different levels of stretch were applied to the tendon to simulate the long-term overuse that causes tendinopathy. At the same time, US images of the tendon were being acquired to measure how the image patterns changed after the stretches had been applied. It was found that radiomic analysis of these patterns was able to detect damage. These findings suggest that quantitative US image analysis could help identify tendinopathy earlier and more reliably than conventional clinical assessments.

Acknowledgements

Table of Contents

List of Figures

List of Tables

Chapter 1: Introduction

1.1   Tendon Anatomy

Tendons are comprised of a hierarchical structure proliferated by the extra-cellular matrix (ECM) of tenocytes. The primary component of the ECM is the tropocollagen molecule, which aggregates into microfibrils, fibrils, and then fibers. Groups of fibers bound together by endotenon are called fascicles, which slide against one another in a nearly frictionless manner. Taken together, the summed collagen structures resist elastic strain and give the tendon ample mechanical strength and toughness under tensile loads [1]. A cross-sectional view of the hierarchical tendon anatomy is shown in Figure 1-1.
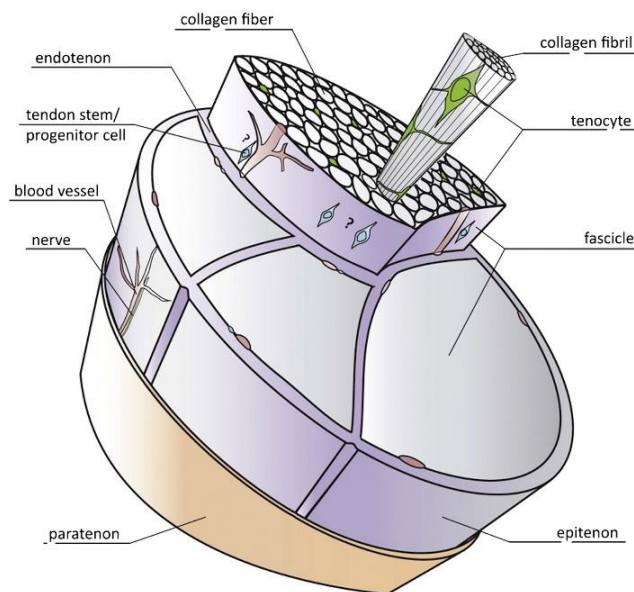
Figure 1-1: A cross-section of a tendon, showing its microstructure, from Docheva et al, [1].

A secondary component of the ECM are glycosaminoglycan (GAG) molecules, which contribute to fluid storage capacity in the tendon. It is thought that the movement of fluid into and out of the tendon is primarily responsible for its fluid-like viscoelastic properties [2, 3]. The hydrophilic GAGs are connected laterally between fibers, contributing to mechanical strength through the formation of hydrated cross-links [3, 4]. Tenocytes have a low metabolic rate [5], which may be a useful adaptation to prevent ischemia and necrosis in a region of large mechanical stresses and relatively little blood flow. However, this trade-off complicates the healing response of tendon, delaying the movement of molecules involved in the inflammatory response and slowing the cell differentiation necessary to replace the collagen matrix at the injury site.

1.2   Tendinopathy

Tendinopathy is a general clinical term used to describe the observed degeneration of the tendon due to chronic overuse, typically resulting in pain, swelling, and reduced performance [6]. Tendinopathy of the Achilles specifically is extremely common among athletes who participate in running and jumping sports [7]. Injury incidence is only exacerbated by higher experience level, with a shocking 43% of elite track and field athletes reporting current or previous symptoms of Achilles tendinopathy (AT), with highest incidence occurring in middle-distance runners, of whom 83% reported past or present symptoms of AT [8]. The injury incidence is high among the general public as well, with only 35% of tendinopathies in a cross-sectional study reported as associated with a sports activity [9]. The exact precursors to tendon injury can be multiple and nuanced, and treatment and recovery can be a lengthy process because tendon is a relatively acellular, avascular tissue. Further complicating effective diagnosis is the reliance on tendon pain as a measure of injury. Previous studies have shown that abnormal, spindle-shaped tendon thickening predicted a greater risk for future development of tendinopathy, even if the tendon was not currently symptomatic [10]. This is owed to the "iceberg theory" of tendinopathy, which states that even severe tendinopathies can remain asymptomatic as overuse damage accumulates such that the pain that is eventually experienced by the patient is only the tip of the proverbial iceberg [11]. As a result, a return-to-activity program based on pain detection threshold does not encapsulate the full depth of accumulated tendon abnormalities, nor does an absence of pain represent complete tendon healing since the significant remainder of the submerged "iceberg" still lingers beneath the threshold of pain. This phenomenon is visualized in Figure 1-2, which shows how overuse damage may accumulate in an asymptomatic case of tendinopathy and how abnormalities are not completely resolved even when no pain is experienced. In order to circumvent this reliance on pain status to classify the damage state of the tendon, *ex vivo* testing was preferred for this experiment.
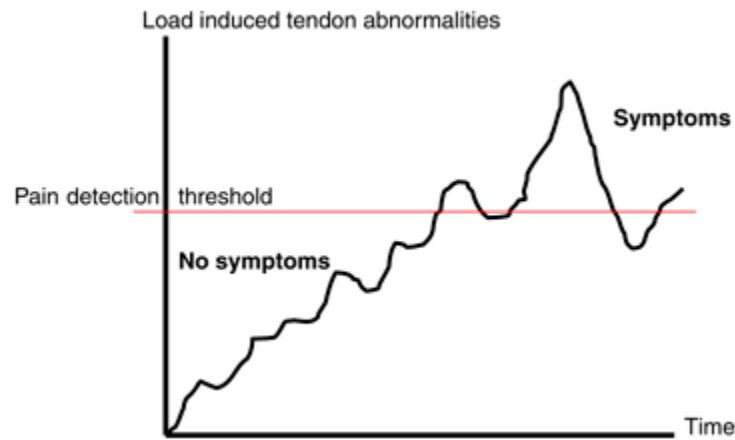
Figure 1-2: A typical injury and recovery timeline for tendinopathy dictated by pain status. After tendon matrix damage has accumulated, inflammation eventually begins to cause pain, stopping activity. Once pain is no longer detected after a period of rest, activity begins again, resulting in continued pain. From Fredberg & Stengaard-Pedersen [11].

In a longitudinal study of soccer athletes, it was demonstrated that ultrasound image abnormalities were strongly predictive of future injury, even if the athlete was asymptomatic at the time of imaging [10]. About 45% of athletes found to have asymptomatic tendon ultrasound abnormalities during preseason were eventually diagnosed with tendinopathy during the season, compared to just 1% of the normal ultrasound group. A meta-analysis supported these results, showing that Achilles tendon abnormalities in baseline imaging were associated with an increased risk of developing tendinopathy [12]. Thus, using ultrasound as an early detection diagnostic tool transcends the challenges of treating an individual based on pain level, which is subject to the iceberg theory. These previous studies indicate the potential for ultrasound to be used in preventative prognoses for at-risk individuals such as athletes and the aging population. The type of tendon matrix degeneration seen in tendinopathy is also an inherent risk factor for a complete rupture, as histologic analysis has suggested that up to 97% of cases of spontaneous rupture exhibit signs of damage and degeneration prior to the rupture event [13]. This further underscores the importance of regular monitoring. Similar methods could also be implemented following an intervention or treatment to evaluate the progression of the healing process. The main barrier to implementation of regular ultrasound screenings, however, is the lack of established quantitative approaches for drawing diagnostic conclusions from these images.

The superficial digital flexor tendon (SDFT) is an energy storing tendon in quadrupeds that has been used as a model for the human AT. As shown in Figure 1-3, the SDFT and the AT are located in anatomically comparable regions. Both also experience high physiological strains, with the AT experiencing peak strains of up to 11.4% while hopping on one leg and equine SDFT

3

straining in excess of 12% during peak gallop [14, 15]. Like Achilles tendinopathy in humans, SDFT injury is the most common tendon and ligament injury (TLI) in racehorses, with an epidemiological study showing that 89% of all TLIs suffered in the study were to the SDFT [16]. Over the course of two seasons, the 1119 racehorses in the study experienced a total of 184 TLIs, showcasing the generally high prevalence of injury. For these reasons, the SDFT was selected for this study as the animal model for the AT. Equine tissue was unavailable for this study, so a porcine model, which has a similar hind limb structure, was selected instead.

Figure 1-3: A comparison of the anatomy of the quadrupedal (left) [17] and human distal limb (right) [18]. The SDFTs in the equine, bovine, porcine, and canine (6 on the diagram) wrap around the calcaneus while the AT inserts at the calcaneus in humans; however, both are vertical, energy-storing tendons that are frequently injured during running activities.

1.3   Biomechanics

The two primary measurements in any assessment of biomechanics are the load applied (P), and the extension observed (ΔL). Structural properties such as stiffness (k) can be measured directly from these two measurements, but they often need to be contextualized by the size of the specimen. Material properties circumvent this challenge by utilizing stress (σ), which normalizes load by the specimen cross-sectional area (A), and strain (ε), which normalizes extension by the initial length of the specimen (L_0). Normalized stiffness is called the elastic modulus (E), which is defined as the ratio between stress and strain. The formula for each of these quantities are shown in Equations 1, 2, 3, and 4 below. In a study involving specimens of varying sizes, material properties are preferred to structural properties since they define the intrinsic characteristics of the specimen, regardless of its geometry.

$$stiffness, k = \frac{P}{\Delta L}$$

Equation 1

$$stress, \sigma = \frac{P}{A}$$

Equation 2

$$strain, \varepsilon = \frac{\Delta L}{L_0}$$

Equation 3

$$modulus, E = \frac{\sigma}{\varepsilon}$$

Equation 4

The stratified and complex structure of tendons results in viscoelastic mechanical behavior. As opposed to traditional solids in which material stress is only related to strain and is independent from time, stress in viscoelastic materials is responsive to strain, strain rate, and duration of strain [19]. Conversely, the magnitude and duration of applied stress can also impact these normalized measures of extension. Further, recovery periods between strain applications can allow viscoelastic materials to regain some stiffness [20]. The most common method for evaluating the tensile mechanical properties of materials is by using a hydraulic or electromechanical testing system and force transducer to apply controlled loads to the specimen and measure extension, or vice versa. Four different test types can be applied to evaluate the unique characteristics of these materials: stress relaxation, creep, cyclic, and pull-to-failure. Characteristic stress-strain (normalized load-extension) plots for each of these tests are shown in Figure 1-4.
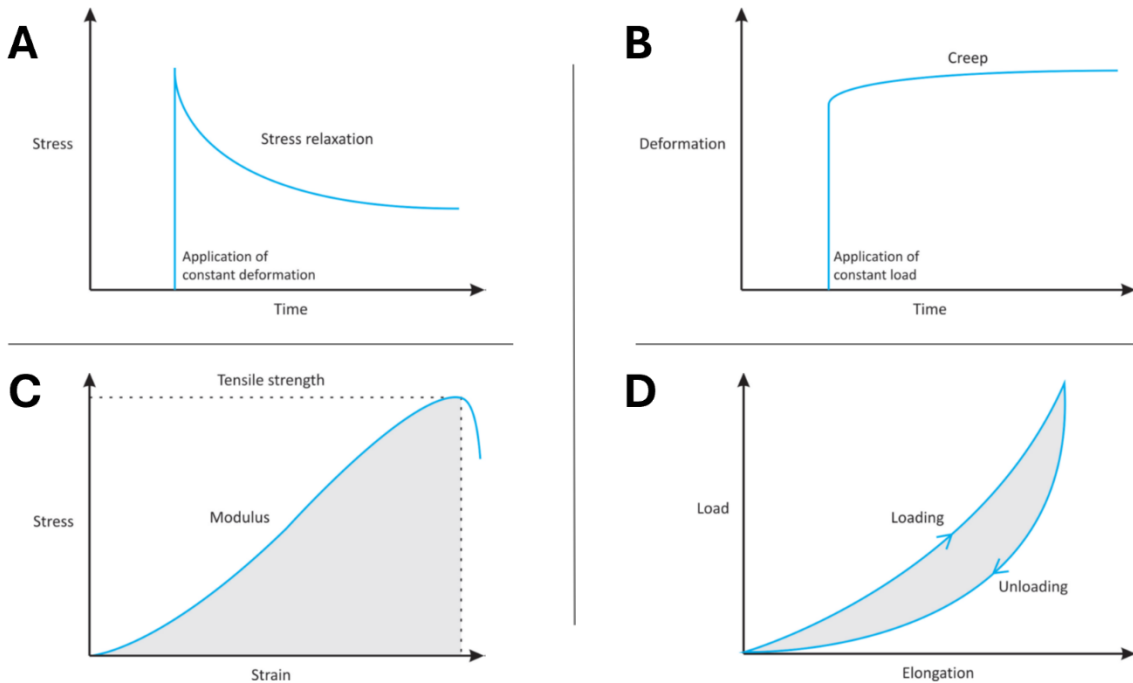
Figure 1-4: Characteristic stress-strain plots of viscoelastic materials tests for (A) stress relaxation, (B) creep, (C) pull-to-failure, and (D) cyclic loading. Adapted from Robi et al [21].

Static stress relaxation is the most common mode of evaluating viscoelastic tendon properties [22]. During this protocol, the electromechanical system gradually extends the specimen

to a specific strain and then holds that strain for a long period, typically between 20-30 minutes. During this period, the load required to hold the strain in the tendon will exponentially decrease (Figure 1-4a). This is because the tendon adapts to this imposed strain and rearranges itself, with individual fibers sliding against one another to better align with the direction of the applied load [23]. The stress relaxation reaches an equilibrium once the fibers have finished sliding and align fully. SDFTs in particular have a large propensity for fiber reorganization compared to non-energy storing tendons, which means the period required for them to reach equilibrium is longer [24]. Alternatively, although not commonly employed in tendon analysis, creep tests are administered by imposing an instantaneous stress and then maintaining it for a long period. Just as stress is impacted by strain, strain rate, and duration of strain, the inverse is also true. Material stresses held for long periods of time cause a characteristic creep curve in which the tendon continues to extend further after the initial stress imposition to a higher equilibrium strain (Figure 1-4b).

Pull-to-failure is a test that is frequently used to destructively evaluate traditional solids as well as viscoelastic materials in which the strain on a specimen is increased at a constant rate until rupture occurs (Figure 1-4c). For viscoelastic materials, there are multiple sections of a typical pull-to-failure plot. The initial period of the test is called the "toe" region and is characterized by a nonlinear, upward concavity curve as additional fibers are engaged in the specimen. This upwardly concave shape corresponds to strain-stiffening behavior, which means the elastic modulus of the specimen is increasing in response to higher strains [25]. As the tendon approaches a point of maximum fiber engagement and therefore maximum modulus, the plot of stress and strain begins to straighten in the "linear" region. Although the yield point is not rigorously defined for nonlinear materials, the point of maximum fiber engagement and maximum stiffness is understood to be the threshold for yield [26], after which additional extension induces strain-softening in the specimen, resulting in lower modulus values within the post-yield region as well as plastic, non-recoverable deformation as the tendon sustains damage. This is marked by a slightly downwardly concave shape on the stress-strain curve. Finally, after the linear region, the modulus sharply declines shortly before the maximum stress is reached. A representation of fiber structure alongside the various landmarks on the pull-to-failure plot is shown in Figure 1-5. Loading the tendon until failure can be instructive, but this method is also inherently destructive and produces significantly different results for instantaneous and equilibrium responses [27].
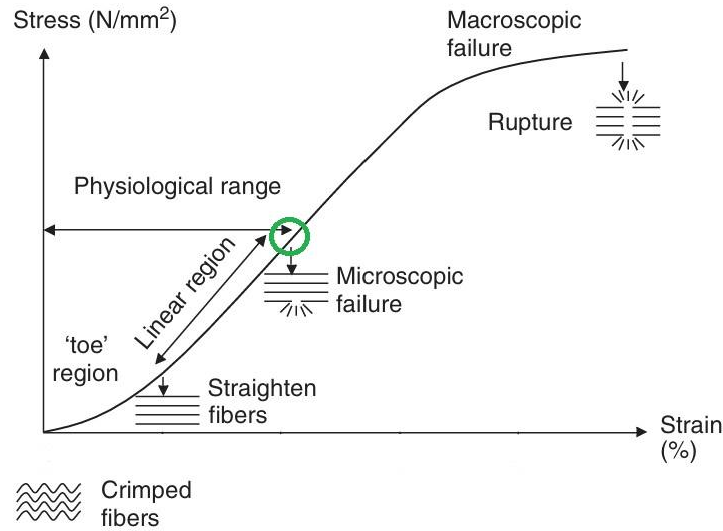
Figure 1-5: A typical stress-strain plot for a tendon pull-to-failure test, labeled with the regional terminology and corresponding fiber behavior at those junctions. The first inflection point of the curve is highlighted with a green circle, corresponding to the yield point. Adapted from Wang [25].

Cyclic loading is typically meant to simulate the physiological behavior of tendons by straining the tendon and returning it to its initial state immediately after. This type of testing forms a hysteresis curve in which the tendon loses between 30-60% of its mechanical energy to heat [28], although the effect level is dependent on strain rate [29]. Figure 1-6 shows a reproduction of Figure 1-4d, illustrating the hysteresis curve on a stress-strain plot, meaning that the area under the curve is measured in [MPa-mm/mm]. A unit conversion yields [J/mm^3], meaning that the area under the loading curve represents the energy per unit volume required to strain the specimen. Consequently, the area under the unloading curve is the energy per unit volume returned by the tendon. Since the volume of the tendon is assumed to be conserved (although load-induced fluid loss in tendon is well-established [2]), the ratio of the area between the loading and unloading curves to the total area under the loading curve is the percentage of energy lost due to heat. This percentage is a material property called hysteresis.
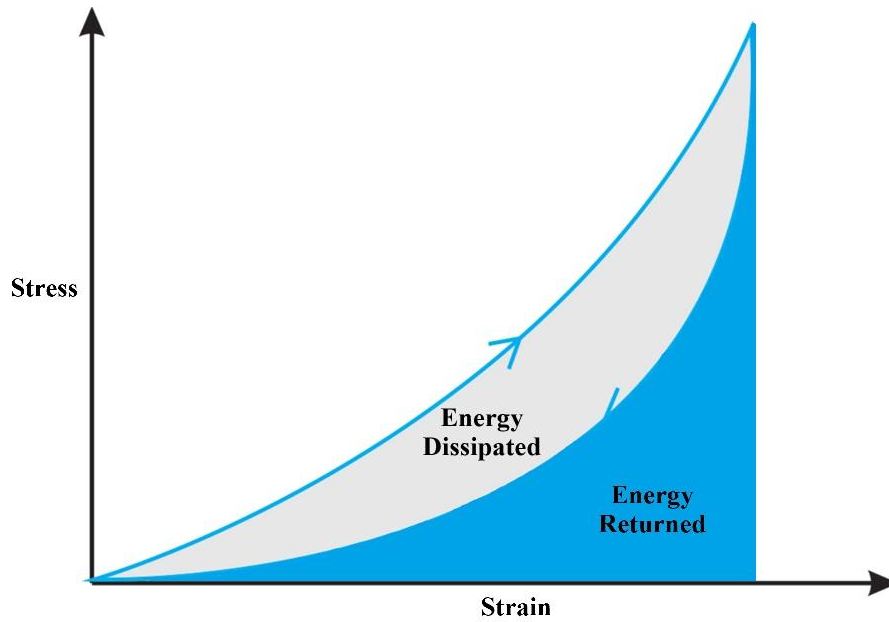
Figure 1-6: A sample hysteresis curve generated from cyclic loading. Hysteresis is calculated as the ratio of Dissipated Energy (gray region) to total energy input (blue and gray region).

Decreased tendon biomechanical properties immediately following these tests are expected, but because part of the decrease is due to sliding fibers under high stresses, a recovery period under no load allows tendons to recover some properties (i.e. modulus and hysteresis) due to fibers returning to their initial positions. Recommendations for the recovery period range from 3 to 10 times the duration of loading [3, 30, 31]. Tendon samples are also commonly preconditioned prior to testing, which has been shown to reduce the confounding effects of viscoelastic properties, allowing the tendon to maintain higher loads during stress relaxations following preconditioning [30]. This is typically done by cyclically loading the tendon at a low stress level for 10-20 cycles.

In the present study, we performed a series of successive stress relaxation tests at progressively increasing strain levels to evaluate the damage sustained by the tendon during the tests. For the purposes of this study, "damage" refers to abnormalities caused by loading events which result in non-recoverable changes to mechanical properties of a tendon. These changes can include an elevation in the minimum tendon displacement required to induce stress, a reduction in the percentage of initial stress that is relaxed during stress relaxation, and a reduction in stress measured for a given strain. This is essentially an extension of the idea of preconditioning, just at a higher loading level. Instead of merely limiting the viscoelastic behavior with preconditioning, a stress applied with the intent to damage the tissue would dissipate it entirely, such that the initial

8

biomechanical properties become unrecoverable even with lengthy rest. There are many different mechanical metrics that can be applied to ascertain that a tendon has experienced damage, although there is disagreement in the literature as to the exact strain level that induces damage, with estimates ranging from 1.5% to 6% strain [20, 23, 32, 33]. Provenzano, et al. introduced a structural damage coefficient D_s defined as the difference in length between preload states applied before (L_0) and after (L_s) a damaging event, normalized by the original length (Equation 6) [32]. As a tendon accumulates damage, its laxity increases, which means it is allowed to strain further without resistance. As a result, applying a nominally low preload to a damaged tendon will cause it to strain further than an undamaged tendon. Tendon laxity can also be increased experimentally by preconditioning, but to a much lesser extent [30].

In a stress relaxation test, E_{eq} is the ratio of the measured stress at equilibrium to the applied strain (Equation 5) [34]. This value is preferred in this study as the true measure of tensile capacity because it is irrespective of the viscoelastic properties of the tendon. Instead, E_{eq} corresponds to the behavior and quality of the collagenous sub-structure of the fibers, which is deteriorated by overload events. While E_{eq} quantifies the quality of the fibers themselves, the percent of the stress that is relaxed (%RLX), that is, the percent decrease in stress during the holding period (Equation 7), can indicate the matrix damage state from between-fiber sliding behavior [24]. Tendons that have experienced more damage will stress relax less than non-damaged tendons [33], although many studies that observe this effect neglect the confounding effect that higher strains have on increased relaxation behavior [31, 35]. The typical stress relaxation figure from Figure 1-4a is represented in Figure 1-7, annotated with the key landmarks used to identify all of these mechanical parameters.
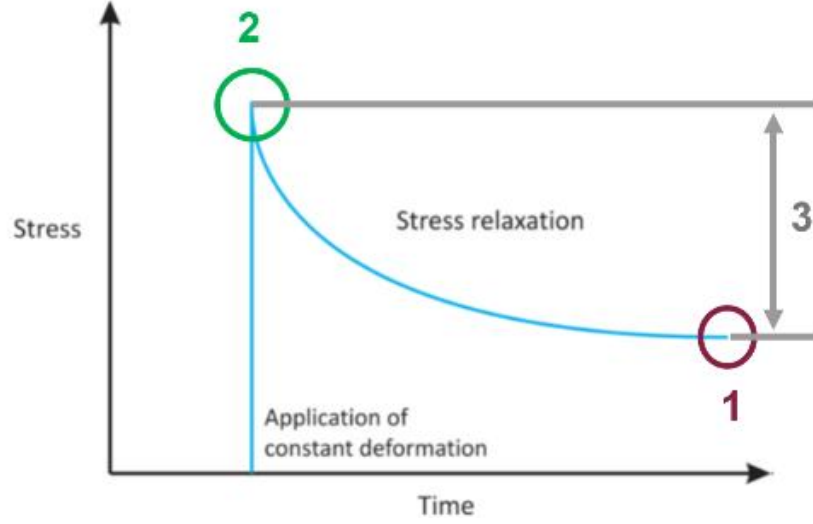
Figure 1-7: A visualization of the points on a typical stress relaxation at which the mechanical parameters of interest are being measured. E_{eq} (1) is the modulus at the equilibrium stress point, D_s (2) is the normalized change in length after damage under identical preloading states, and %RLX (3) is the viscoelastic reduction in stress under fixed strain.

$$E_{eq} = \frac{\sigma_{eq}}{\varepsilon_{eq}}$$

Equation 5

$$D_s = \frac{L_s - L_0}{L_0}$$

Equation 6

$$\%RLX = \frac{\sigma_{max} - \sigma_{eq}}{\sigma_{max}}$$

Equation 7

1.4   Ultrasound

Ultrasound imaging is a widely used, non-invasive diagnostic tool for soft tissue injury. For a typical diagnosis, a sonic signal transducer is placed against the skin of the patient with a gel coupling medium, sending supersonic waves into the body which are then reflected back to the transducer. An ultrasound image (UI) is then reconstructed from the spatial intensity of the returning waves, creating a two-dimensional picture of the structures immediately beneath the skin. Ultrasound waves are outside of the range of human hearing, classified as frequencies above 20 kHz, although medical probes typically operate between 1 and 20 MHz [36]. Higher frequencies allow for better resolution but are more likely to be attenuated by the tissue, resulting in poorer imaging penetration depth. Conversely, images acquired using lower frequencies have worse resolution, but do provide improved imaging penetration depth, producing a larger image [36]. The intensity of the returning wave, also called the echogenicity, is quantized into 8 bits, so the resulting value of each pixel within the reconstructed UI ranges from 0 to 255. Accordingly, high brightness regions are hyperechoic, while low brightness regions are hypoechoic. Healthy tendon exhibits a pattern of bright, hyperechoic striations from aligned collagen fibers, while tendinopathy is

10

indicated by dark, hypoechoic regions within the tissue from fiber disarray [37]. Hypoechogenicity along with other imaging hallmarks of tendinopathy such as visible disruption of fibers, blurring along tendon margins, and neovascularity are shown in Figure 1-8 [38]. It has been demonstrated that US, as opposed to magnetic resonance imaging (MRI), has a greater accuracy in confirming clinical diagnosis of tendinopathy [39]. In addition to providing a higher spatial resolution, an inherent advantage of using US is that the two-dimensional image slice can be focused towards the problematic region, whereas MRI slices are more random and may exclude areas of interest within the space between slices. Incidentally, although both modalities are non-invasive and do not involve exposure to radiation, US images are far less expensive and time-consuming to acquire [40], an important consideration for both research and clinical settings.

a) Hypoechoic changes within proximal tendon

b) Fibrillar disruption in the posterior proximal tendon

c) Marginal blurring along posterior proximal tendon

d) Doppler showing neovascularity
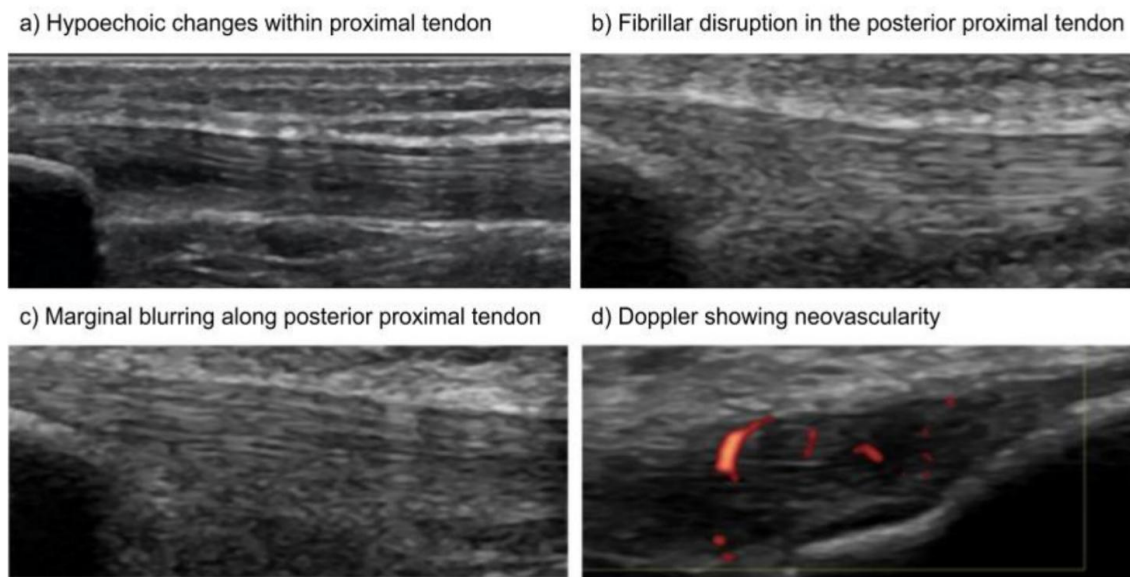
Figure 1-8: Clinical indicators of tendinopathy from a US image of a patellar tendon, from Mitchell [38].

In the clinical setting, tendon damage is assessed using semi-quantitative grading scales such as the Öhberg scale, which rates patient tendon health on a scale of 0-3, with 0 indicating normal structure and 3 indicating severe structural changes. Clinicians primarily look for qualitative changes such as those in Figure 1-8 and then rate the severity of the change on the Öhberg scale [41]. However, even between experienced clinicians, there is usually a lack of agreement between ratings and the distinction between levels is somewhat vague [42]. Even quantitative measures taken from ultrasound images such as tendon thickness suggest systematic differences between radiologists [43]. These circumstances suggest a need for more robust quantitative approaches to tendon health evaluation.

11

1.5   Texture Analysis

Radiomics is the extraction of numerical values from medical images for clinical decision-making. Texture analysis (TA), a subset of radiomics, is the process of using algorithms to quantitatively examine the shade, alignment, and distribution of UIs to assess the disease state of a tissue or organ [44-46]. The simplest TA methods to implement are statistical approaches, which comprise a broad category of features. First-order features are derived from a frequency histogram, summarizing the central tendency of pixel intensities in the image, and include mean, variance, skewness (i.e., tendency towards low or high value outliers), and kurtosis (i.e., sharpness of histogram peak) [47]. It should be noted that the order of the parameter in the context of TA is not related to its statistical exponential order, in which kurtosis is considered fourth order. Instead, the order of the feature is in reference to the number of pixels being considered.

Accordingly, second-order features account for spatial variation between 2 pixels in the form of the gray-level co-occurrence matrix (GLCM). The features extracted from the GLCM are also referred to as Haralick features, from the author who first described them [48]. The GLCM is a square matrix with size equivalent to the number of pixel intensity levels present in the original image [49], which corresponds to a 256 x 256 matrix for an image quantized into 8 bits. The value of each GLCM matrix position value is encoded by the number of times a pixel of intensity denoted by the column number is adjacent to a pixel of intensity denoted by the row number [44]. This encoding process is visualized in Figure 1-9, with (a) and (c) representing the numerical and visual representations of the original image, respectively, and (b) and (d) representing the same for the GLCM. In this example, there are 4 pairs of the pixel values 1 and 6, meaning that position (1, 6) has a value of 4 in the GLCM. In a 2D image, each pixel has 2 neighbors in each of 4 angles, $\theta = 0°$ (vertical), $\theta = 90°$ (horizontal), $\theta = 45°$ (up-diagonal), and $\theta = 135°$ (down-diagonal), resulting in 8-connectivity. As a result, four GLCMs are generated, encoding the frequency in which pixel pairs occur for a given angle. Parameters are calculated from the formulas listed in Table 1 for each angular GLCM and the mean value of the four angular parameters is returned. Model-based approaches have shown that GLCM Correlation is an effective measure of collagen fiber orderliness [50]. A greater amount of waviness and disarray present in an image corresponds to lower measures of correlation.
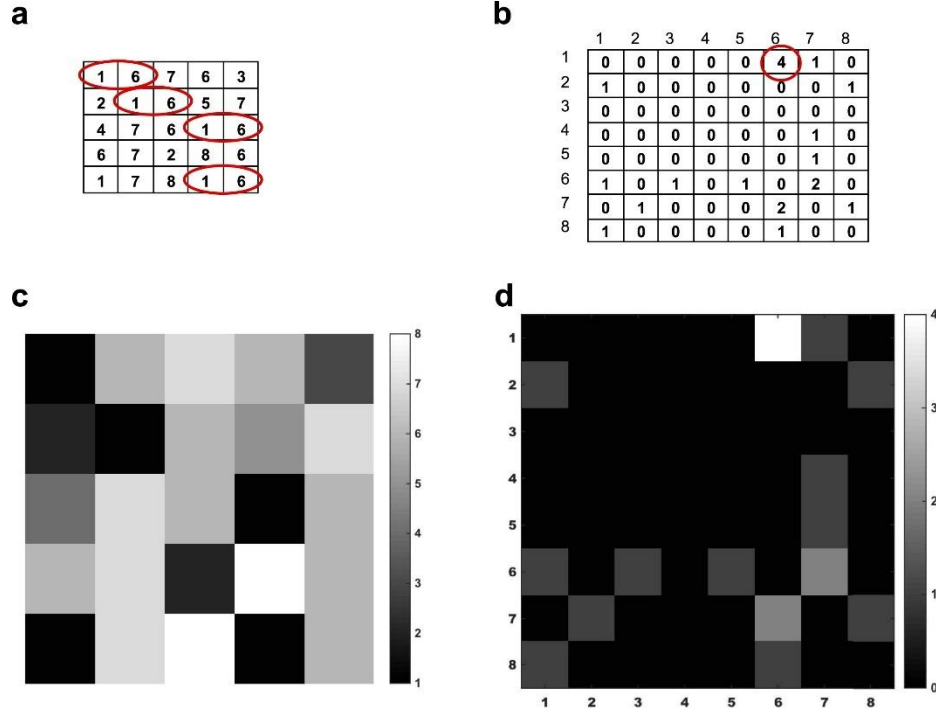
Figure 1-9: The construction of the $\theta = 0°$ gray-level co-occurrence matrix (GLCM) (b, d), from the original image (c) and its quantitative pixel intensities (a) to illustrate trends in neighboring pixels. Figure from Molinari et al, [49].

Prior clinical studies of first- and second-order texture analysis have shown it is capable of identifying pathology-induced differences in tissue structure and composition; the results are compiled in Table 1 [51-54]. For clarity, there are both first- and second-order parameters termed entropy and energy [44, 49], but only the second-order GLCM parameters are listed here. Further confusing matters, the first-order energy parameter is also occasionally referred to as uniformity [55].

Table 1: Directional association for First- and Second-Order TA Features in the presence of tendinopathy. N = 256, the number of pixel values possible; (x, y) refers to the pixel position in the original image; (i, j) refers to a matrix position.

Texture Parameter	Formula	Description	Order	Δ with pathology	Ref.
Mean	$\mu = \dfrac{1}{MN}\displaystyle\sum_{x=1}^{M}\sum_{y=1}^{N} A(x,y)$	Average pixel value.	1st	Decrease	[51-54]
Variance	$\sigma^2 = \dfrac{1}{MN}\displaystyle\sum_{x=1}^{M}\sum_{y=1}^{N} (A(x,y) - \mu)^2$	Dispersion of pixel values around the mean.	1st	Unclear	[51, 53, 54]
Skewness	$\dfrac{1}{MN\sigma^3}\displaystyle\sum_{x=1}^{M}\sum_{y=1}^{N} (A(x,y) - \mu)^3$	Asymmetry in the distribution of pixel values.	1st	Increase	[51, 53, 54]

Kurtosis	$\dfrac{1}{MN\sigma^4}\displaystyle\sum_{x=1}^{M}\sum_{y=1}^{N}(A(x,y)-\mu)^4$	Concentration of the distribution of pixel values near the mean.	1st	Increase	[51, 53, 54]
GLCM Mean	$\mu_i = \displaystyle\sum_{i,j=0}^{N-1} i(P(i,j))$	Average pixel value of the GLCM.	2nd	Not typically reported	
GLCM Variance	$\sigma_i^2 = \displaystyle\sum_{i,j=0}^{N-1} P(i,j)\,(i-\mu_i)^2$	Dispersion of GLCM pixel values around the GLCM mean	2nd	Not typically reported	
Entropy	$-\displaystyle\sum_{i,j=0}^{N-1} P(i,j)\log_2 P(i,j)$	Disorder within the tendon. Considers the number and proportions of grayscale levels.	2nd	Decrease	[51, 54]
Energy (ASM)	$\displaystyle\sum_{i,j=0}^{N-1} P(i,j)^2$	Consistency of patterns in the GLCM.	2nd	Increase	[54]
Contrast	$\displaystyle\sum_{i,j=0}^{N-1} (i-j)^2 P(i,j)$	Local variation between neighboring pixels.	2nd	Decrease	[53, 54]
Homogeneity	$\displaystyle\sum_{i,j=0}^{N-1} \dfrac{1}{1+(i-j)^2}P(i,j)$	Local similarity between neighboring pixels.	2nd	Increase	[52-54]
Correlation	$\displaystyle\sum_{i,j=0}^{N-1} P(i,j)\left[\dfrac{(i-\mu_i)(i-\mu_j)}{\sqrt{(\sigma_i^2)(\sigma_j^2)}}\right]$	Fiber orderliness. A larger degree of waviness and disarray corresponds to lower correlation.	2nd	Decrease	[56, 57]

Higher order features consider 3 or more pixels, typically in the form of pixel "neighborhoods" consisting of the 1 or 2 pixels surrounding a given point in any direction or adjacent pixels with equivalent values. One example of the former is the Neighborhood Gray-Tone Difference Matrix (NGTDM) which evaluates the similarity between a pixel and its 8 surrounding neighbors using Equation 8 [58].

$$\bar{A}_i = \bar{A}(k,l) = \frac{1}{W-1}\left[\sum_{m=-d}^{d}\sum_{n=-d}^{d} f(k+m, l+n)\right]$$

Equation 8

f(k, l) is the gray value for the pixel at (k, l), d specifies the radius of the neighborhood around the pixel, and $W = (2d+1)^2$, representing the overall number of pixel values in the neighborhood including the central value. Dividing the summed neighborhood pixel values by the neighborhood size generates the average surrounding pixel value, $\bar{A}_i$. Equation 9 subtracts that average surrounding value from the value of the center pixel and sums the result for every pixel at the same gray level in the entire image [58].

$$s(i) = \sum \left| i - \overline{A}_i \right|$$

Pixel values, i, with low s(i) outputs are surrounded by pixels of similar shade, while high s(i) outputs indicate hotspots – sharp changes in echogenicity between neighboring pixels. The most important and straightforward meta-statistic from the NGTDM is coarseness, which is defined as a high degree of local uniformity. Mathematically, this is represented as the inverse of the sum of all the entries in the NGTDM multiplied by a small probability correction factor. Large coarseness values are expected to indicate tendon damage by expressing similarity between neighboring pixels absent the characteristic bright striation pattern from organized, healthy collagen fibers.

Higher order parameters that encapsulate 1-dimensional runs of identical pixel values or areas of identical pixel values include the outputs of gray-level run-length matrix (GLRLM) [59], gray-level size matrix (GLSZM), and blob analyses, which have also been shown to be capable of identifying pathology-induced differences in tissue structure and composition [60]. The binary segmentation morphology techniques detailed in Section 2.3.2 are another example of higher order feature implementation.

The gray-level dependence matrix (GLDM) was developed as a computationally efficient method to resolve the angular dependency of the GLCM [61]. Briefly, the GLDM quantifies gray level dependencies, defined as the number of connected pixels that are equivalent to the center pixel in an 8-connectivity neighborhood. Each row represents a possible gray level, while each column represents a number of possible dependencies, resulting in a 256 x 8 matrix. The matrix value at position (i, j) is the number of pixels in the image at gray level i that had j dependent neighbors. Therefore, in an image with large, homogeneous objects, the GLDM will be populated with higher values towards the right-hand side due to larger dependency counts. The GLDM is distinct from the NGTDM because it only registers pixel neighbors with the same value but only does so at a distance of 1, unlike the GLRLM and GLSZM.

Acquiring comparable images is dependent on effective and consistent probe operation, which is frequently challenging because of unclear anatomical reference points [62]. Standardization becomes more difficult when considering the other factors involved in probe operation, including measuring with correct acoustic power and gain level, probe pressure on the skin, and the positioning of the patient, which can affect the angle of the ultrasonic wave. Figure

1.9 demonstrates an exaggerated instance of the latter, as maximal internal shoulder rotation is required to properly image the supraspinatus tendon since it does not appear in the neutral position, despite no change in probe positioning. From this, it is clear that even small changes in diagnostic procedure can compromise the resulting image composition. Previous *in vivo* studies of texture analysis have noted the large variation of texture features between UIs, likely due to small changes in ultrasound transducer operation or minute movement of anatomical structures [53].
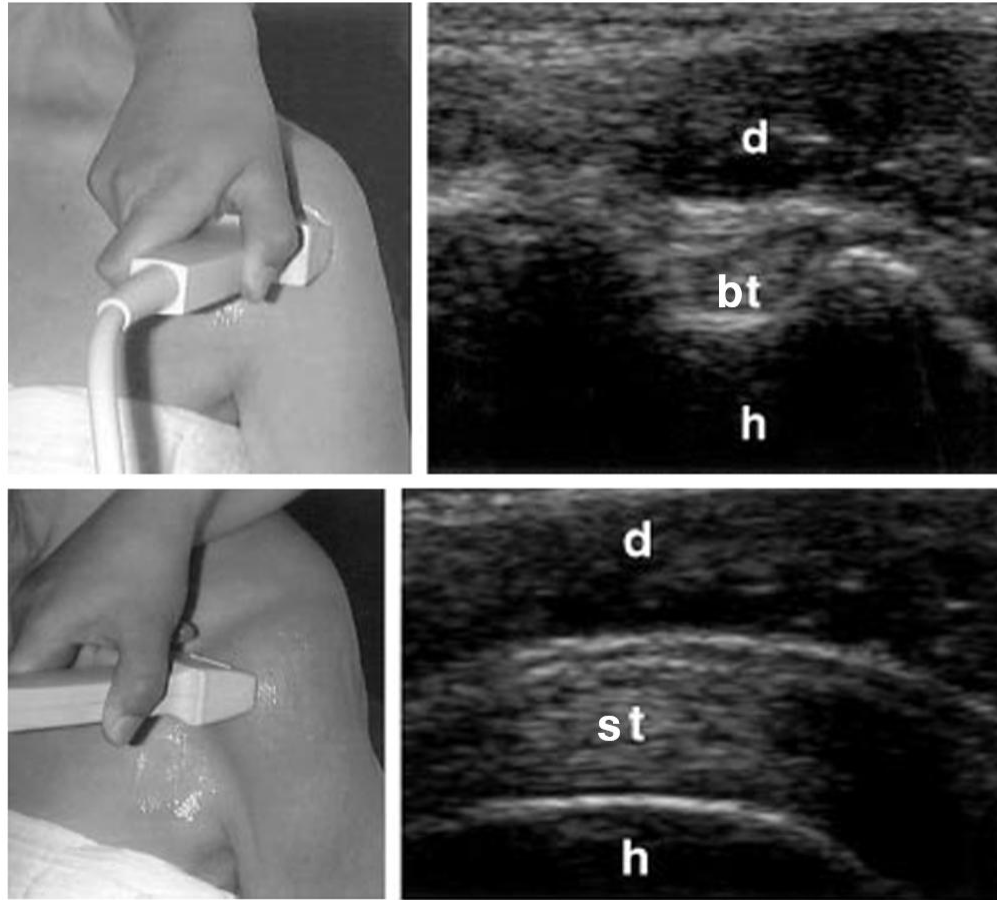
Figure 1-10: Comparison of UIs acquired of the shoulder. Although probe positioning is unchanged, an entirely different tendon is brought into view upon internal shoulder rotation. h = humerus; bt = biceps tendon; st = supraspinatus tendon; d = deltoid muscle. Adapted from Backhaus, et al. [62].

To circumvent this limitation, imaging of an *ex vivo* tendon will be conducted in this study. This further allows for the controlled loading and simultaneous imaging of tendon. Previous studies have examined differences in echogenicity in *ex vivo* tendons under mechanical loading. Duenwald et al. found that porcine SDFTs exhibited higher echogenicity under higher applied strains and stresses [63]. This corresponded with the findings from Schmidt, who utilized high-cycle fatigue testing in cadaveric Achilles tendons and found that samples that exhibited higher

strain not only had higher mean echogenicity but were more likely to experience rupture during testing [64]. However, Duenwald and colleagues later found that the effect of strain on echogenicity was less pronounced in tendons that had experienced an overstretch similar to the Damage Ramp implemented in this study (See Section 2.2.4) [65]. Synthesizing these previous studies yields apparently opposite outcomes with regard to the relationship between tendon integrity and mean echogenicity. This inconsistency in echogenicity predictive power suggests that it represents an incomplete measure of tendon health and damage state. Texture analysis is capable of discerning greater detail from ultrasound imaging than mean echogenicity alone. Indeed, Riggin et al. used a non-texture based method that would not likely be replicable in a clinical setting to analyze collagen fiber alignment and found that tendon damage reduced fiber alignment [66]. Verification of texture analysis in assessing tendinopathy could extend these results to a more generally applicable method.

1.6   Specific Aims

Aim 1: Determine the threshold of quasi-static strain magnitude that induces mechanical damage in porcine superficial digital flexor tendons. This will be quantified by a series of progressively increasing held strains. Reduction in Modulus and % Relaxation as well as an increase in Laxity following a given strain would be considered evidence of damage, establishing that strain level as the damage threshold. **Our objective is to evaluate the change induced in porcine SDFT mechanical properties resulting from a series of progressively increasing applied strains.**

Aim 2: Investigate how radiomic parameters change after a tendon has experienced one or several damaging events. By implementing imaging and loading concurrently, this experiment will quantify changes to the tendon texture and radiomic indices in response to loading. Two distinct protocols will be used in separate groups to quantify damage. **It is expected that tendon ultrasound texture parameters will differ significantly following loading and between different tensile strain levels.**

Chapter 2: Methods

2.1 Sample Preparation

Nine healthy juvenile female pigs were sacrificed for other projects in accordance with IACUC standards and all hind limbs were frozen upon sacrifice and transported to the lab at Virginia Tech (Blacksburg, VA) from Wake Forest School of Medicine (Winston-Salem, NC). Limbs were subsequently thawed and dissected to remove the SDFT, as shown in Figure 2-2 and Figure 2-1. Upon removal, tendon samples were wrapped in saline-soaked gauze and placed in a plastic bag before entering a -20°C freezer until the day of testing. The full SDFT dissection protocol is available in Appendix A – Dissection Protocol.
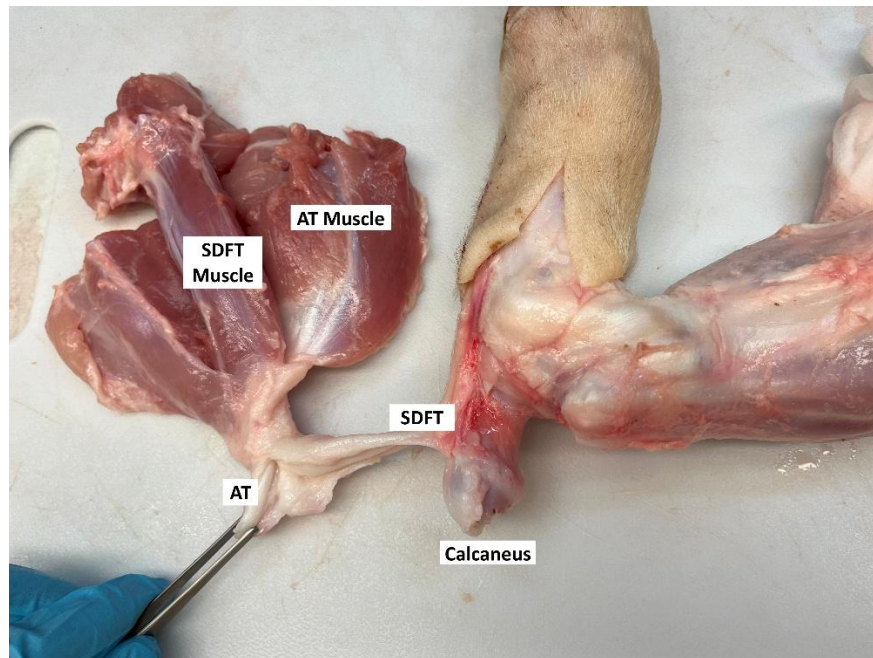
Figure 2-1: A dissected porcine hindlimb illustrating the location of various tendon and muscle structures associated with the dissection of the SDFT.

On the day of testing, the bagged and wrapped tendons were placed in a lukewarm water bath for 30 minutes. Following thawing, a size 11 scalpel was used to remove any additional muscle tissue from the proximal end of the specimen. Width (w) and thickness (t) measurements of the medial portion of the tendon were taken three times using calipers and averaged to estimate an elliptical cross-sectional area using the formula $A = \frac{\pi}{4} wt$.

2.2 Mechanical Testing

2.2.1 Testing Setup

The biomechanical loading was carried out using a Material Test System Insight 10 loading frame (MTS) with a 5 kN load cell. The full walkthrough of the various procedures used to carry out mechanical testing on the MTS is included in Appendix B – MTS Test Protocol. The tendon was gripped using two sandpaper-covered metal plates and fixed to a gripping mount already in place on the MTS. A polycarbonate (PCA) tank (Figure 2-3) was installed around the test area to be filled with approximately 10 L of 0.9% saline. The saline-filled tank serves two purposes. First, the lengthy nature of the test necessitates constant hydration of the tendon, and second, the supersonic signal associated with ultrasound imaging is least attenuated by a liquid medium [67]. A compression seal was applied between the tank and the test platen by using a slip joint coupling. A custom ultrasound probe mount was placed inside the tank to monitor the tendon under load (Figure 2-4). Multiple angles of the fully assembled testing setup with the tendon gripped in place are shown in Figure 2-5 prior to filling the tank with saline.
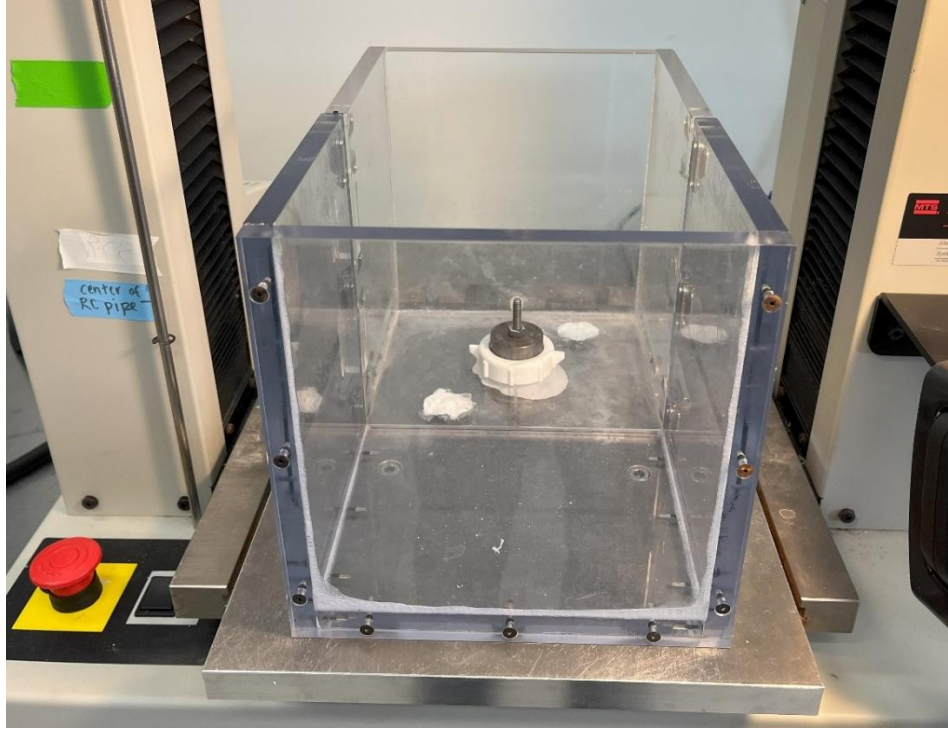
Figure 2-3: A polycarbonate tank was installed around the tendon loading area to hold a 0.9% saline solution, facilitating US image acquisition and maintaining tendon hydration. A hole was cut from the tank for the test platen, so a slip-joint coupling is applied on the platen for sealing at this junction.
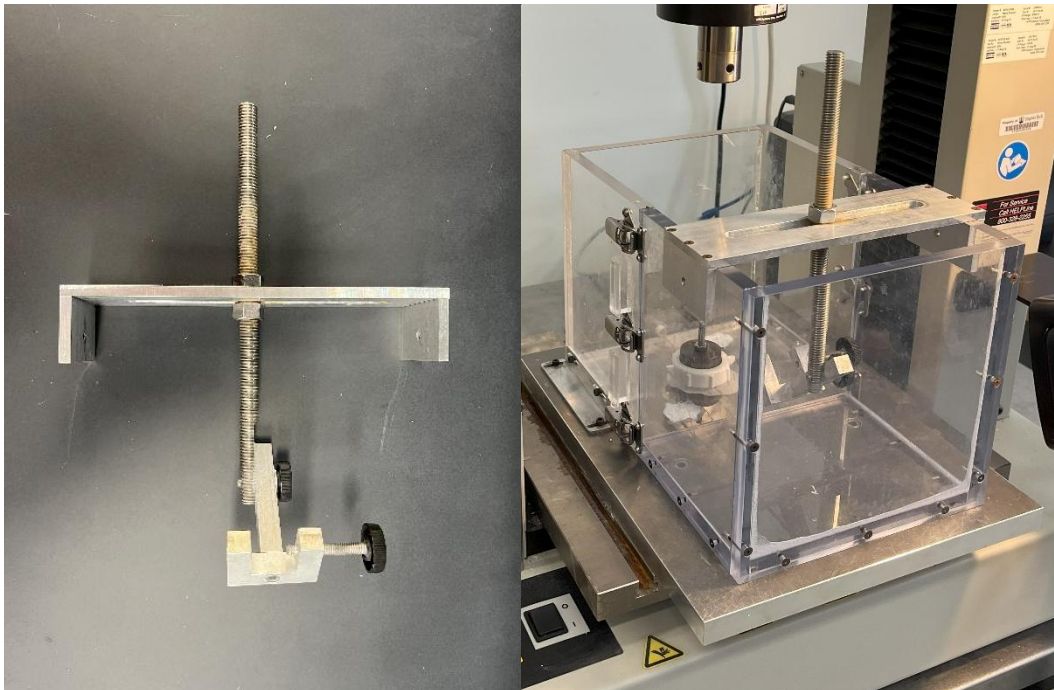
Figure 2-4: A custom fixture to hold the clinical US probe during testing, mounted on the tank.
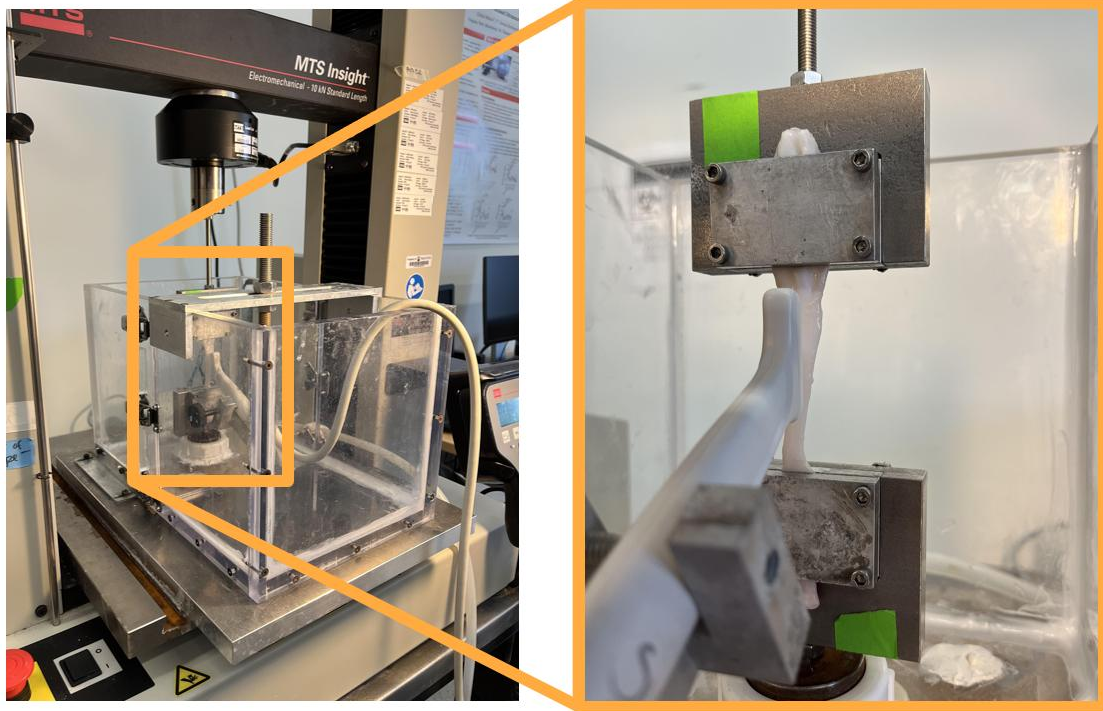
2.2.2 Preconditioning

With the tendon grips and US probe in place, the load cell was zeroed after filling the tank since a slight buoyant effect of the saline on the steel gripping fixtures was observed. Prior to any testing, the tissues were preloaded to 2 N and then held at the extension required to initially achieve this load for 3 minutes, inducing a slight stress relaxation in the sample to ~1 N. All tendons then immediately proceeded into a preconditioning period of 20 cycles at 0.5 mm/s between 2 N and 4 N. After preconditioning, the tendon was allowed to rest for 5 minutes before proceeding to testing.

2.2.3 Protocol 1 – Progressive Stress Relaxation

The objective of this set of tests was to ascertain the strain that induces damage in the tissue matrix during a long hold to allow transient viscoelastic properties to dissipate. The primary parameter of interest for this biomechanical experiment was the equilibrium modulus (E_{eq}), which was determined by the change in stress at equilibrium with respect to the imposed strain. The SDFTs designated to the Progressive Stress Relaxation group (n = 6) were subjected to the protocol shown in Figure 2-6. A preload of 2 N was applied for 3 minutes before each strain level imposition to reduce viscoelastic effects and provide a taut state for consistent imaging. The tendons in this

group experienced strain levels of 2, 4, 6, and 8 percent, in that order. The tissue extensions associated with each strain level were calculated by the MTS program with respect to the adjusted gage length, that is, the length of the specimen after applying the 2 N preload. That way, the tendon would start each level from a baseline taut state. Each strain level was held for 25 minutes to allow ample time to reach equilibrium and then returned to zero load for 20 minutes. After the final strain level and recovery period, the tendon was again preloaded to 2 N at a rate of 0.5 mm/s and held at that extension for 3 minutes, then pulled at a rate of 0.5 mm/s until failure was achieved as a residual strength test. During this residual strength test, sample failure was specifically defined by a 90% reduction from peak load during the pull-to-failure. This ensured that complete fibrillar failure had taken place, even if there was no visible rupture.
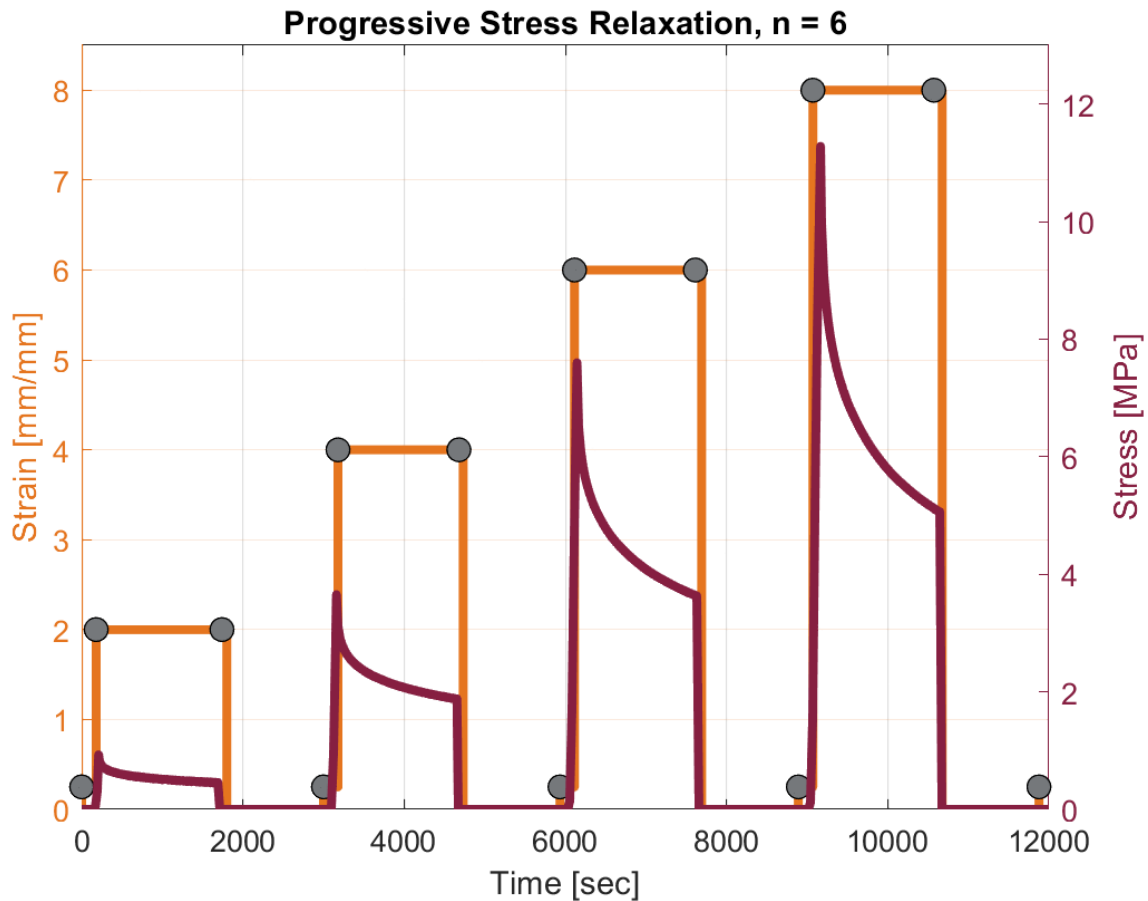
Figure 2-6: A representative figure of the stress measured during the Stress Relaxation protocol. For simplicity, the periods spent in preload and the final pull-to-failure were excluded from this figure.

Stress and strain data were acquired by the MTS during each of the stress relaxations as well as the pull-to-failure. Plotting stress against strain during the stress relaxations generated

hysteresis-like curves for the stress relaxations at each strain level. were plotted on top of one another with lines drawn between equilibrium points, representing E_{eq} for that interval. A custom MATLAB script (MATLAB R2024b, The Mathworks, Inc., Natick, MA, USA) was used to extract the relevant mechanical parameters – E_{eq}, Laxity, and % Relaxation – from the stress relaxation data. A separate script calculated residual yield stress, yield strain, elastic modulus for the pull-to-failure. Both are included in Appendix C – Mechanical Analysis Code.

2.2.4 Protocol 2 – Damage Ramp

The objective of this set of tests was to measure the effect of a single high-stress damage event, in contrast to a lengthy period of overuse, on tendon biomechanical properties. The tissues designated to the Damage Ramp group (n = 8) were subjected to the protocol shown in Figure 2-7. As with Protocol 1, tendons were preloaded at 2 N for 3 minutes before each major load application to dissipate viscoelastic effects. Section 2.2.3 as well as previous literature suggested that 2% strain level would not induce damage, so a stress relaxation test was repeated before and after the damage ramp to ascertain E_{eq}. On the other end of the spectrum, a 10% strain level is generally accepted as above the level at which damage occurs, but well below ultimate failure strain (15-20%) [33], so this strain was chosen as the peak target for the damage ramp.

Logistically, samples were preloaded, strained to 2 percent at 0.5 mm/s and held for 20 minutes and then allowed to recover under zero load for 20 minutes. Next, samples were preloaded again, pulled to 10% at a rate of 5 mm/s and immediately returned to zero load for another 20 minutes. Finally, the samples were preloaded and strained to 2 percent for 20 minutes again.
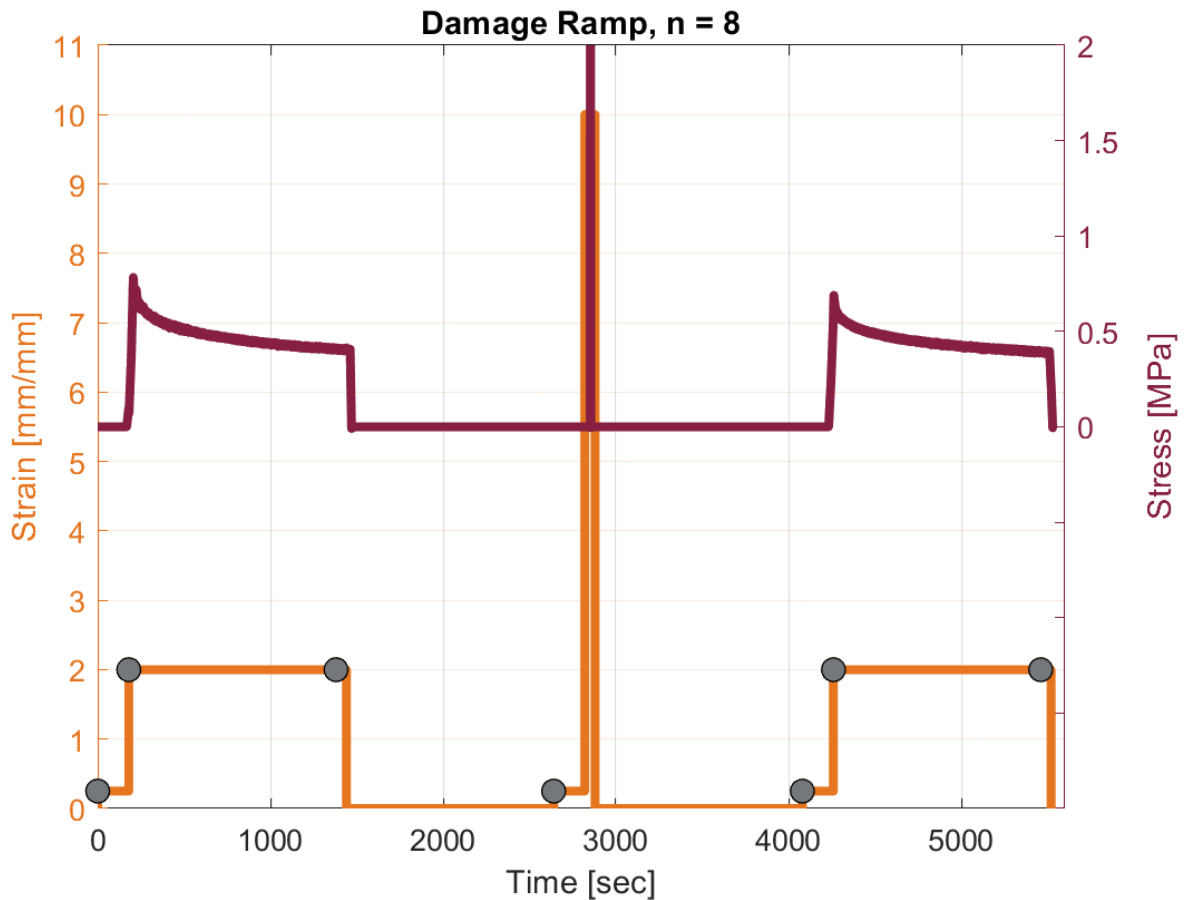
Figure 2-7: A visual schematic of the Damage Ramp mechanical protocol. Imaging points are labeled with gray dots. Orange plot denotes strain application and maroon plot denotes measured stress.

Due to the high strain rate used during the damage ramp, the viscoelastic damping properties of the tendon induced a large degree of hysteresis. This is visualized in a representative plot from SDFT sample #1 in Figure 2-8. Similar figures for the other 7 samples are included in Appendix D – Additional Figures. The peak stiffness occurs at the first inflection point of the curve, identified at 4.63% strain. According to Peloquin, the peak stiffness also corresponds to the yield point of the specimen [26].
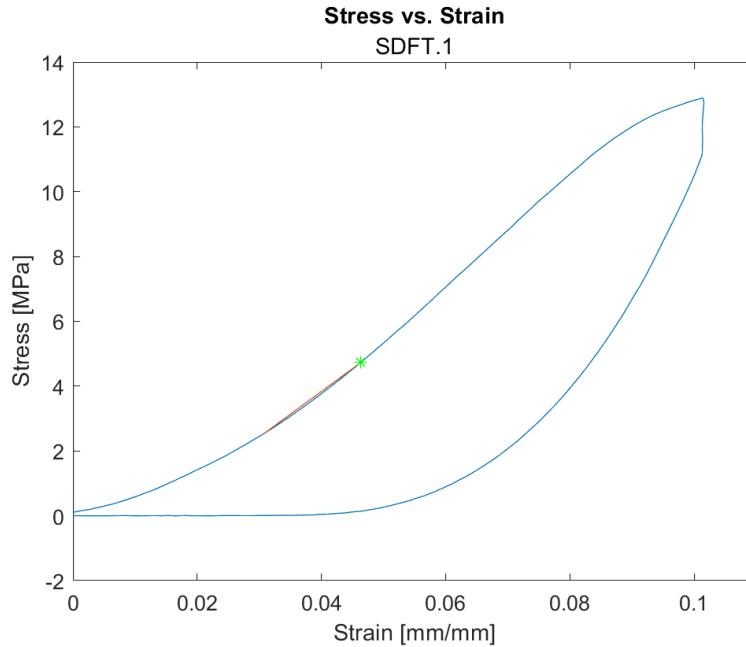
Figure 2-8: Hysteresis curve for the damage ramp to 10% strain. The green marker denotes detection of specimen yielding due to maximum stiffness being reached at 4.63% strain.

As with Protocol 1, stress and strain data were acquired by the MTS during each of the stress relaxations as well as the damage ramp. In this case only Laxity and % Relaxation were calculated from the stress relaxation data. Using Peloquin's definition, yield stress, yield strain, and elastic modulus were calculated for the damage ramp, as well as hysteresis.

2.3 Sonographic Imaging

2.3.1 Image Acquisition

US images were acquired using an Aixplorer Supersonic Imagine clinical machine (Hologic, Inc., Marlborough, MA) with the SLH20-6 linear probe. Acquisition took place throughout the mechanical testing protocol to assess the correlation between image texture and mechanical properties. Images were always acquired while the tendon was under a nonzero load to avoid irregularities in image analysis with slackened tendons. A diagram of the overall workflow for the experiment is shown in Figure 2-9.
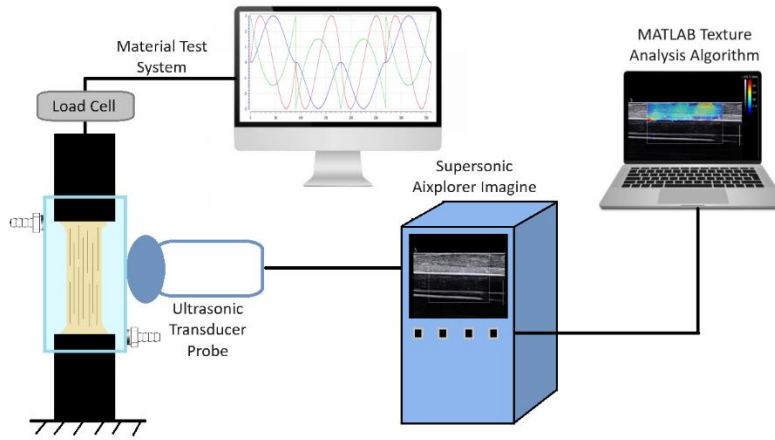
Figure 2-9: Diagram of the entire experimental setup.

2.3.2 Image Analysis

Images were exported from the clinical machine in DICOM format and subsequently read into NumPy arrays using the python-dicom and gdcm libraries. B-mode images were thresholded using pixel brightness, creating binary masks of the tendon. Pixel thresholding takes all of the pixel values above a certain value and logs them in a separate binary .png mask file as a 1, with all other pixel locations registered as a 0. This creates a binary image mask that can then be applied to the original image during analysis to determine which values to "keep" because they have been classified as part of the tendon. Additional morphological operations were also applied to the sample to ensure the entire tendon sample was included in the automatic segmentation. These simple operations evaluate the 8-pixel neighborhood around a point to smooth the edges of the thresholded mask as shown in Figure 2-10, and have been implemented in medical image analysis since at least the 1980s [68]. Dilation replaces the central pixel in the neighborhood with a 1 if any of the surrounding pixels are also 1, swelling the mask coverage when applied to the entire spatial pixel set iteratively. Conversely, erosion replaces the central pixel with a 0 if any of the surrounding pixels are also 0, shrinking the overall mask. For this image set, three binary erosions were conducted, followed by two binary dilations. Next, a hole filling operation was performed, which further replaced any binary 0 regions in the mask with 1 if it was surrounded by 1's. Finally, each unconnected component of the eroded and dilated binary mask was labeled and only the largest component was kept, which efficiently removed all smaller particles that passed through the pixel threshold such as bubbles in the imaging medium and image echo artifacts.
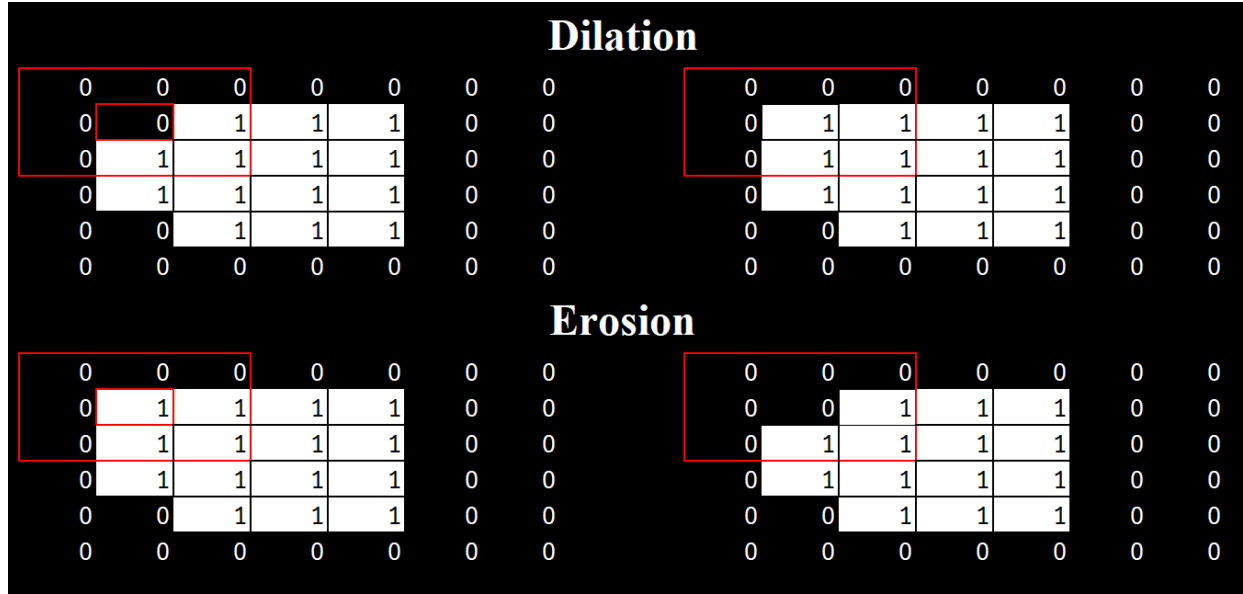
Figure 2-10: Sample of morphological operation used to smooth edges of US image binary masks after applying pixel thresholding.

Due to the *ex vivo* nature of the test, this automated segmentation protocol was sufficient to isolate the tendon from the background. The automated segmentation was verified by implementing the Dice-Sorensen coefficient to assess inter- and intra-user variability between the automated segmentation and manual users, adapting the methodology from Zijdenbos, et al. to compare a manual and semiautomatic binary segmentation of medical images [69]. Each manual segmenter completed two segments of each of the US images from SDFT sample #17. The Dice-Sorensen coefficient was then calculated between and within users by utilizing the dice() function in MATLAB, a sample output of which is shown in Figure 2-11. The formula for the coefficient is simply twice the number of pixels common to both segmentations divided by the sum of the sizes of both segmentations, producing a value between 0 and 1.

$$0 \leq DSC = \frac{2|A \cap B|}{|A| + |B|} \leq 1$$

Equation 10

The mean Dice-Sorensen coefficient of the 7 images in the reliability test are shown in Table 2, with each row and column displaying the initials of the segmenter or the pixel threshold used in the automatic segmentation. Although segments generally improved in agreement in concordance with increasing pixel threshold value, a visual inspection of the 110-pixel threshold showed significant absences in the automated segment of the tendon. Additionally, the implementation of the erosion and dilation morphological operations detailed above further improved the 100-pixel

27

threshold Dice-Sorensen coefficients to match that of the 110-pixel threshold. As a result, the default automated segmentation protocol for all US images in this work utilized a 100-pixel value threshold as well as morphological operations. SDFT #15 had multiple images not load properly under this protocol, so a 65-pixel threshold was used instead, along with morphological operations. SDFT #8 was inundated with bubbles, so a manual segmentation was carried out for each image in that set.
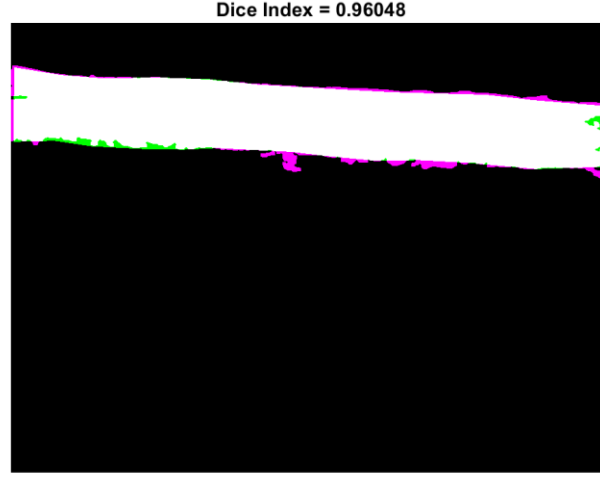
Figure 2-11: A sample output from the MATLAB dice() function. White regions are areas of agreement between segmenters, green regions were selected by only the human segmenter, and pink regions were selected by only the automated segmenter.

	BB1	BB2	KC1	KC2	SH1	SH2	Auto 50	Auto 80	Auto 100	Auto 100 w/morph	Auto 110
BB1		0.98	0.96	0.97	0.97	0.97	0.89	0.92	0.94	0.95	0.95
BB2			0.96	0.97	0.97	0.97	0.91	0.93	0.95	0.96	0.96
KC1				0.97	0.95	0.96	0.87	0.90	0.93	0.94	0.94
KC2					0.96	0.96	0.88	0.91	0.93	0.94	0.94
SH1						0.98	0.91	0.93	0.95	0.96	0.96
SH2							0.90	0.93	0.95	0.96	0.95
Auto 50T								0.97			

Table 2: Dice-Sorensen coefficient values for manual and automatic segmentations of SDFT #17. Bold values indicate intra-user reliability measures.

After applying B-mode image masks, a gray level histogram was constructed for each US image acquired at preload, from which first-order parameters were generated. Next, a GLCM, GLDM, GLRLM, GLSZM, and NGTDM were also constructed for each image. Then, radiomic

parameters were generated based on these second and higher order matrices by the pyradiomics library [70]. Between first, second, and higher order, a total of 93 radiomic parameters were generated for each image. These parameters follow definitions described by the Imaging Biomarker Standardization Institute (IBSI), an initiative that seeks to standardize the definitions and reference values used in radiomics for improved clinical decision making [55]. The python scripts used in this study to segment the images, generate histograms and matrices, and calculate texture parameters are included in Appendix E – Radiomic Analysis Code.

2.4 Statistical Analysis

A mixed effects model was applied to all mechanical and textural parameters from US images taken at preload generated from the progressive stress relaxation with the strain level as a fixed effect and the tendon sample number as well as the crossed factor between tendon sample number and strain level as random effects. The fixed effect had 4 or 5 levels (initial for images only as well as 2, 4, 6, and 8), so a post hoc Tukey's Honest Significant Difference (HSD) test was used to assess differences among group means. Another mixed effects model was applied for the mechanical and textural parameters from US images taken at preload generated from the damage ramp, with pre- and post-damage ramp as a fixed effect and the tendon sample number as well as the crossed factor between tendon sample number and pre- and post-damage ramp as random effects. All models were fit using JMP Student Edition 18 (SAS Institute Inc., Cary, NC).

Chapter 3: Results

3.1 Biomechanical Properties

3.1.1 Protocol 1 – Progressive Stress Relaxation

The damage accumulated in the tendon was quantified by three parameters calculated from the preload and stress relaxation data: E_{eq}, D_s, and % Relaxation. A representative plot of the hysteresis-like curves from the stress relaxation testing of SDFT sample #15 is shown in Figure 3-1. Similar plots for the other 5 tendons are included in Appendix D – Additional Figures. Figure 3-2 and Figure 3-3 show direct comparisons between the laxity parameter, D_s, and % Relaxation, respectively.
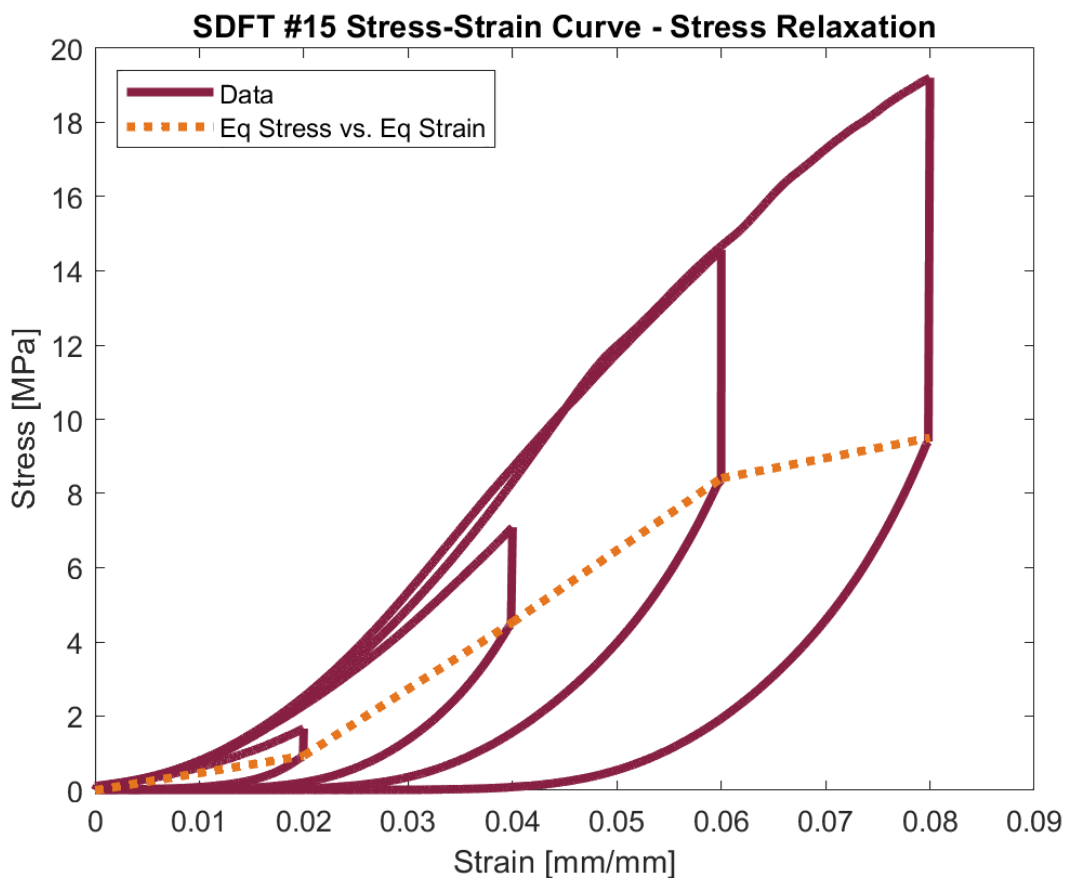
Figure 3-1: Stress-Strain plot of a full progressive stress relaxation protocol with Equilibrium Modulus (E_{eq}) plotted across equilibrium stresses. Note the crossover between the ramps to 6% and 8%, indicating changes in slope during the ramp – evidence of post-yield behavior.

Tendon Laxity after each Strain Level
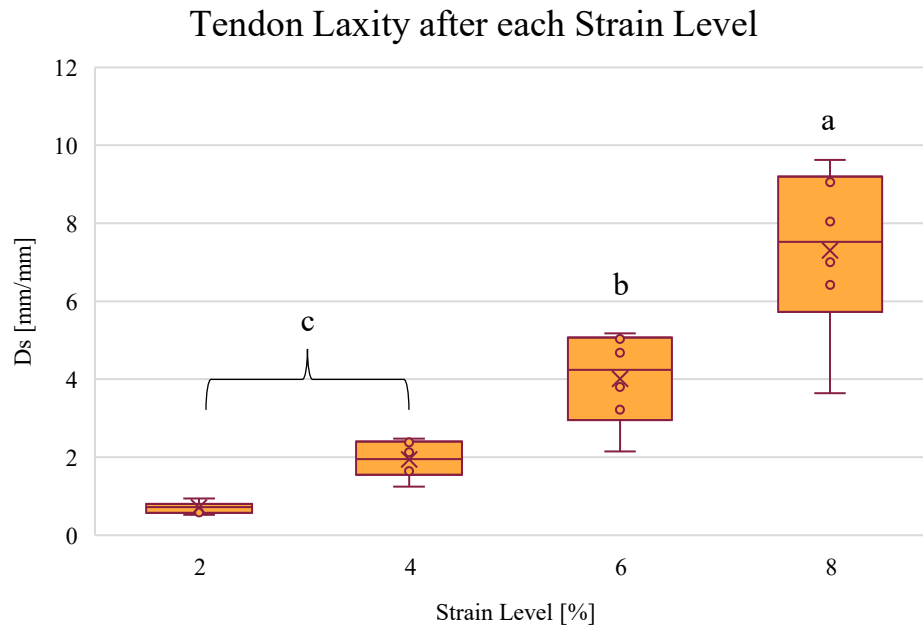
Figure 3-2: Measures of tendon laxity at preload following a stress relaxation and recovery at each strain level. Strains were held for 25 minutes, followed by 20 minutes in slack for recovery before assessment at preload. Levels not labeled with the same letter are significantly different.

% Relaxation during each Strain Level
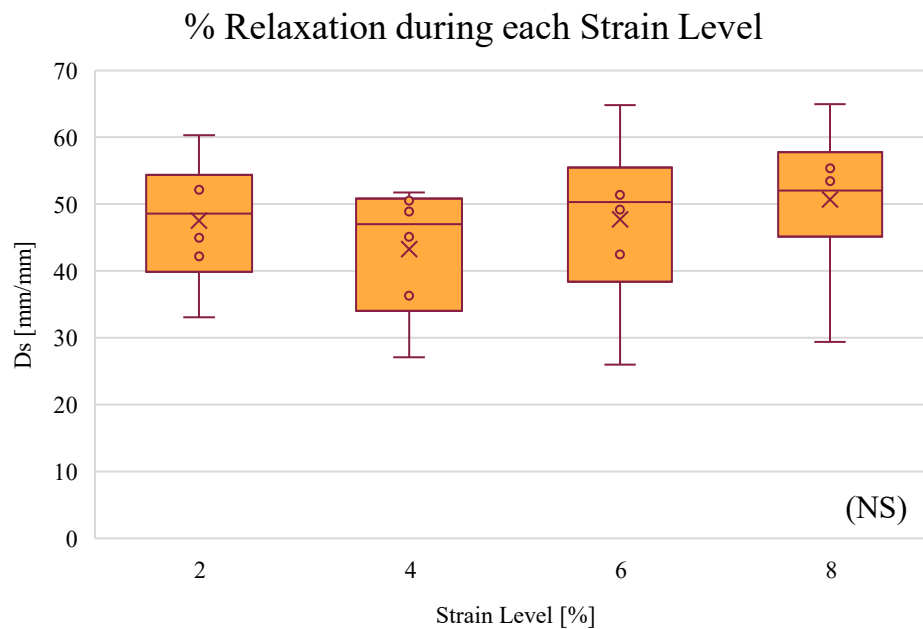
Figure 3-3: Measures of the percent decrease in stress during the course of the 25-minute strain hold for each strain level. No significant differences were observed between groups.

The results for the three parameters across the 4 strain levels are compiled in Table 3.

Strain Level	Laxity (D_s) [mm/mm]	% Relaxed	Equilibrium Modulus (E_{eq}) [MPa]
2	0.708 ± 0.148	47.5 ± 9.52	32.5 ± 15.8
4	1.94 ± 0.472	43.3 ± 9.69	98.5 ± 53.7
6	4.01 ± 1.18	47.7 ± 12.9	109 ± 71.1
8	7.30 ± 2.16	50.7 ± 11.7	78.3 ± 51.8

3.1.2 Protocol 2 – Damage Ramp

For the tendons that experienced the damage ramp, the three mechanical parameters were measured before and after the 10% strain damage ramp. Both were significantly different after the ramp, as shown in Figure 3-4 and Figure 3-5.
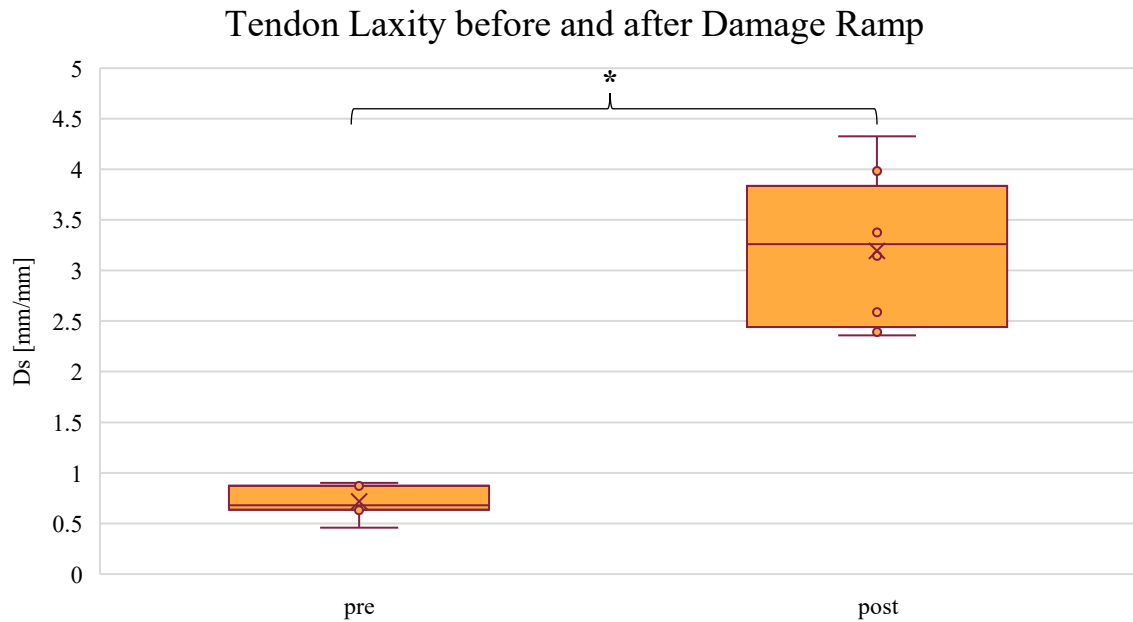
Figure 3-4: Comparison of the tendon laxity parameter (D_s) prior to and following the 10% strain damage ramp.

32
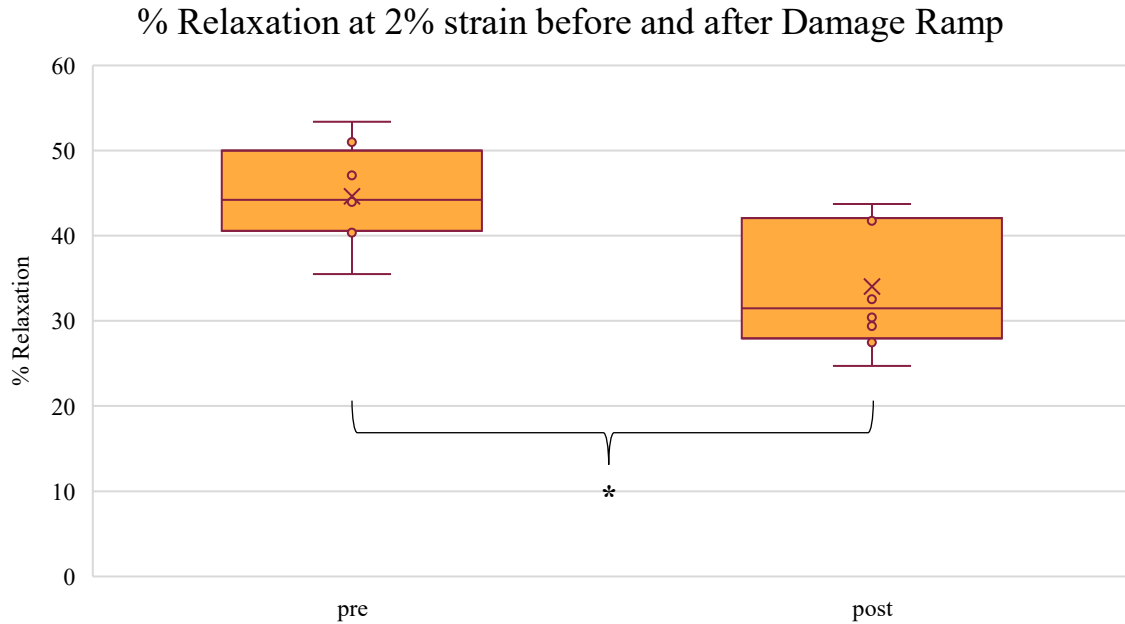
Figure 3-5: Comparison of the percentage of stress relaxed at 2% strain prior to and following the 10% strain damage ramp.

Mechanical data acquisition was conducted during the damage ramp as well as the residual strength test to assess more traditionally reported properties such as modulus, yield stress and strain, and percent energy loss due to hysteresis. SDFT samples #2 and #14 exhibited no yielding during the damage ramp and were excluded from this analysis. The results of these analyses are listed below in Table 4.

Table 4: Mean and SD of key traditional mechanical properties from analysis of ramp to 10% strain and residual strength test following progressive stress relaxation.

Test Type	Yield Stress [MPa]	Yield Strain [mm/mm]	Modulus [MPa]	Energy Loss Ratio
Damage Pull	12.57 ± 8.40	0.0529 ± 0.0090	252.61 ± 79.09	0.55 ± 0.08
Post-Stress Relaxation Pull-to-Failure	6.42 ± 1.85	0.0427 ± 0.0049	232.66 ± 79.15	N/A

3.2   Sonographic Analysis

3.2.1 Protocol 1 – Progressive Stress Relaxation

A progression of US images taken at preload of SDFT sample #13 following stress relaxations at the indicated strain levels are shown in Figure 3-6. Although the sample appears

relatively similar after the 2% strain level to the initial state, further deterioration is evident after imposing the additional strain levels. Like in clinical cases of tendinopathy, fibrillar disruption and marginal blurring – a lack of the bright white edge marking the edge of the tendon – are evident in the images taken after the 6% and 8% strain levels.
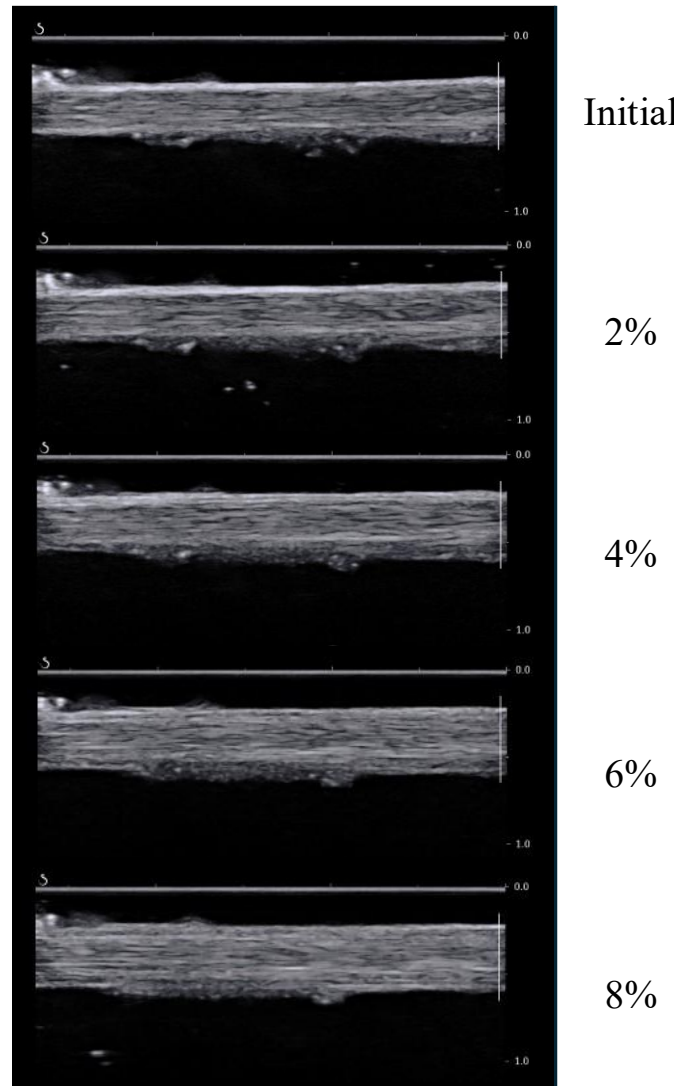
Figure 3-6: Progression of US images taken at preload of SDFT sample #13 following the strain levels at the right of each image. Higher strain levels induce greater fibrillar disruption and reduced edge brightness, which could manifest in vivo *as marginal blurring.*

In total, 31 of the 93 texture parameters from the pyradiomics library were found to have at least one significant difference between groups. This was visually consistent with the deterioration seen in the Upon further review of Tukey's HSD results for each parameter, 13 of those 31 were capable of distinguishing between 3 strain levels. Table 5 shows those parameters that were sensitive to loading history for the Progressive Stress Relaxation tests.

Table 5: Texture Parameters capable of distinguishing between 3 strain levels.

Parameter Type	Matrix Origin	Order	Prob > F
Coarseness	NGTDM	>2	<0.0001
Gray Level Non-Uniformity	GLRLM	>2	<0.0001
Gray Level Non-Uniformity	GLSZM	>2	<0.0001
Gray Level Non-Uniformity, Normalized	GLRLM	>2	0.0003
Gray Level Non-Uniformity, Normalized	GLSZM	>2	0.0003
Dependence Non-Uniformity	GLDM	>2	0.0012
Informational Measure of Correlation 1	GLCM	2	<0.0001
Informational Measure of Correlation 2	GLCM	2	0.0001
Joint Energy (Angular Second Moment)	GLCM	2	0.0007
Run Entropy	GLRLM	>2	0.0021
Zone Entropy	GLSZM	>2	0.0021
Entropy	First Order	1	0.0006
Uniformity	First Order	1	0.0004

Joint Entropy and Sum Entropy from GLCM as well as Dependence Entropy and Gray Level Non-Uniformity from GLDM were also significant but only distinguished between two connected levels in a Tukey's HSD test. Including these four additional parameters, the most sensitive texture parameters to tendon strain level fall into four categories: coarseness, uniformity, correlation, and entropy. Selected parameters from each of these categories are shown in Figures 3-7 through 3-10 to illustrate the progression of changes with damage level. Notably, each type of gray level matrix as well as the first order gray level frequency histogram are represented by at least one significant parameter.

Gray-Level Non-Uniformity at preload - GLDM
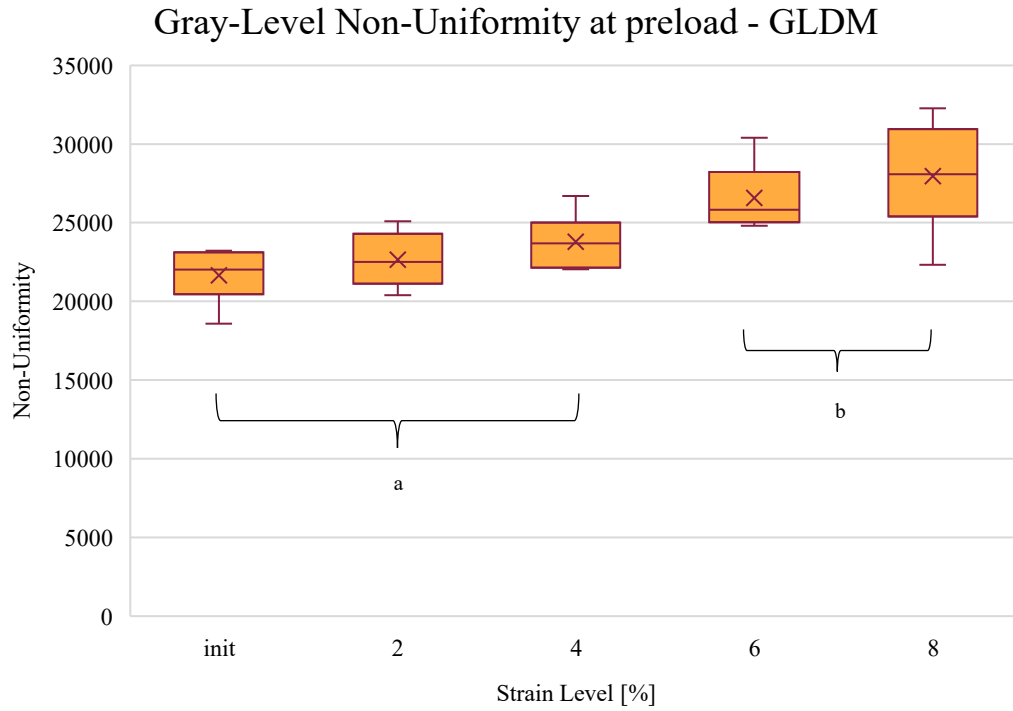
Figure 3-7: The texture parameter gray-level non-uniformity, as calculated from the gray-level dependence matrix (GLDM) at preload after the progressive strain levels.

Coarseness at preload - NGTDM
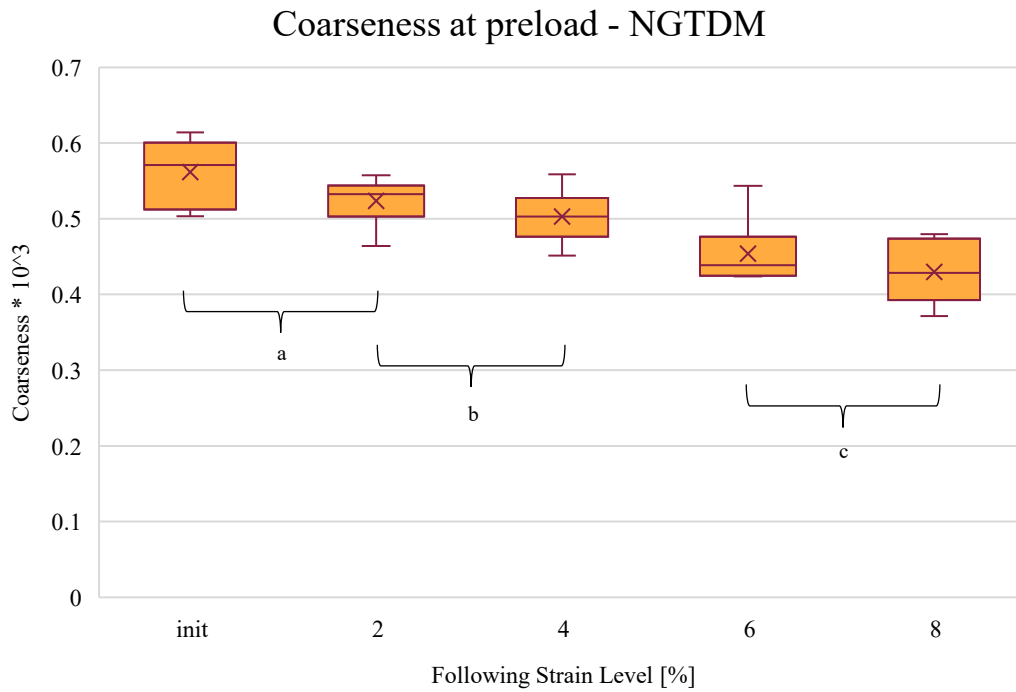
Figure 3-8: The texture parameter Coarseness generated from the neighborhood gray-level difference matrix (NGTDM) after each strain level had been experienced.
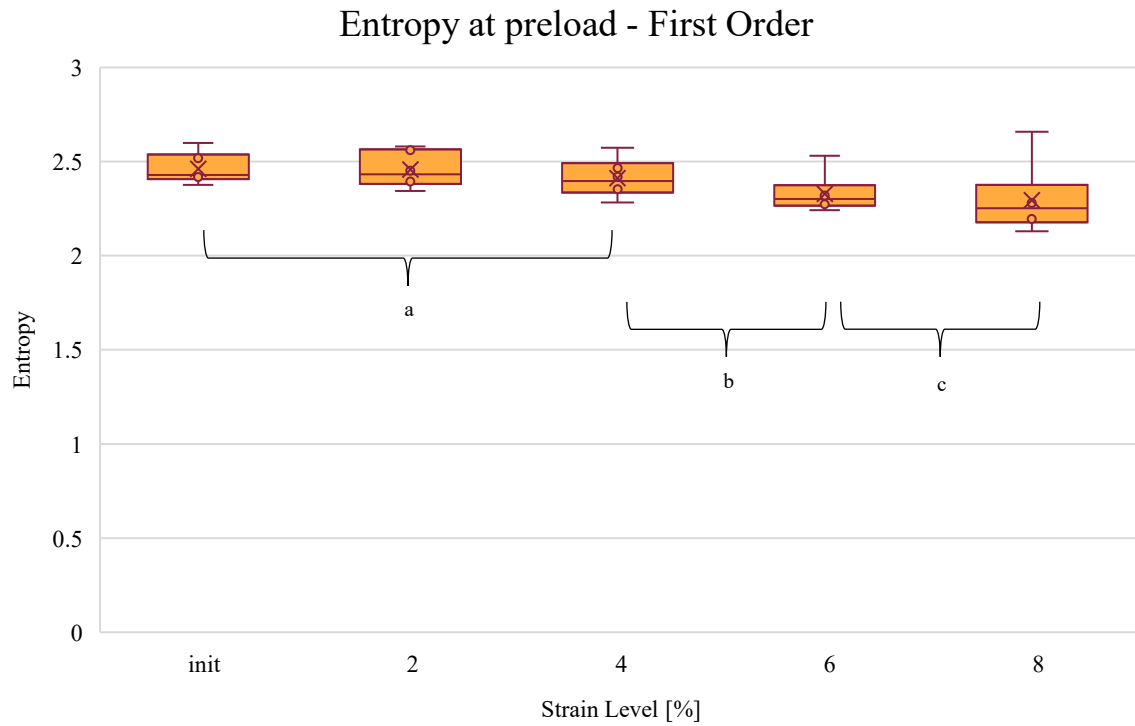
Figure 3-9: The texture parameter Entropy generated from the first order gray-level frequency histogram after each strain level had been experienced.
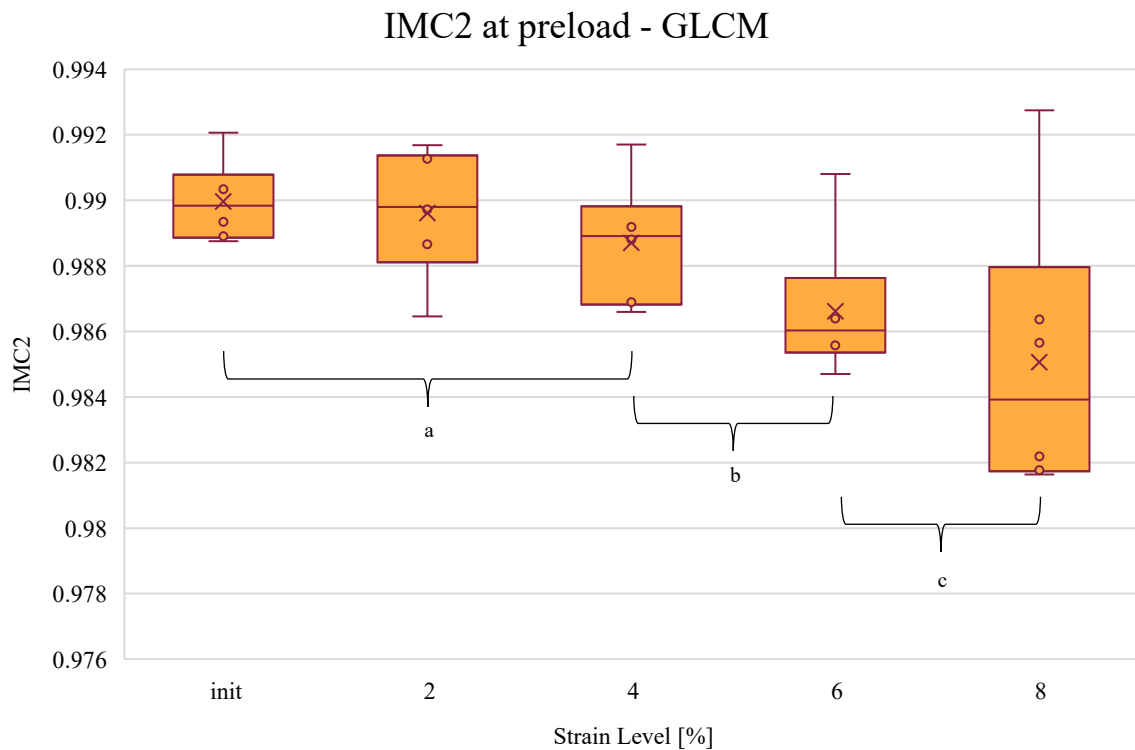
Figure 3-10: The texture parameter Informational Measure of Correlation 2 generated from the gray-level co-occurrence matrix (GLCM) after each strain level had been experienced.

37

3.2.2 Protocol 2 – Damage Ramp

10 of the 91 texture parameters were found to be significantly different after the 10% strain damage ramp. Those parameters are compiled in Table 6.

Table 6: Texture parameters capable of distinguishing tendon before or after damage ramp.

Parameter Type	Matrix Origin	Order	Prob > F
Coarseness	NGTDM	>2	0.0225
Gray Level Non-Uniformity	GLDM	>2	0.0039
Gray Level Non-Uniformity	GLRLM	>2	0.0127
Gray Level Non-Uniformity	GLSZM	>2	0.0127
Gray Level Non-Uniformity, Normalized	GLRLM	>2	0.0094
Gray Level Non-Uniformity, Normalized	GLSZM	>2	0.0094
Gray Level Variance	GLRLM	>2	0.0251
Gray Level Variance	GLSZM	>2	0.0251
Robust Mean Absolute Deviation	First Order	1	0.0322
Mean Absolute Deviation	First Order	1	0.0439

Chapter 4: Discussion

4.1 Biomechanical Properties

4.1.1 Protocol 1 – Progressive Stress Relaxation

The main objective of this set of tests was to fulfill Aim 1 and ascertain the strain level that induces damage in the SDFT when held for an extended period. Three parameters (E_{eq}, D_s, and %Rlx) were compared before, during, or after applying each of four progressively larger strains to the samples. It was expected that if damage had occurred in the sample during the testing, E_{eq} and %Rlx would decrease, while D_s would increase. Two of those three outcomes occurred after the 6% strain had been applied.

In the stress relaxation tests, the reduction in E_{eq} after 6% strain was seen as evidence of damage in the tissue. Although the equilibrium stress was necessarily higher for higher strain levels, the change in equilibrium stress was lower between 6% and 8% strain after remaining relatively linear between 2% and 6%. This corresponds to what is typically seen during a monotonic pull-to-failure, which has a lower stiffness toe region up until ~2% strain from tendon fiber uncrimping, a linear region between 2% and 6% strain, and macroscopic failure beginning to occur after that point, denoted by a reduction in tangential modulus, as shown in Figure 4-1 [25]. E_{eq} has been used frequently as a proxy for elastic modulus in viscoelastic specimens, specifically when quantifying the behavior of fibers in lieu of the overall matrix. Previous studies have examined E_{eq} within a single fascicle as opposed to the tendon as a complete unit [23, 71]. This result suggests that single fascicle mechanical behavior largely mimics that of the full-sized tendon in stress relaxation testing. Mow observed a long linear region of E_{eq} in quasi-static compression testing of cartilage up to -20% strain [72]. While both represent mechanical tests of collagenous tissue, collagen type and direction of testing (tensile vs. compression) clearly differentiate the results of this experiment and Mow's.
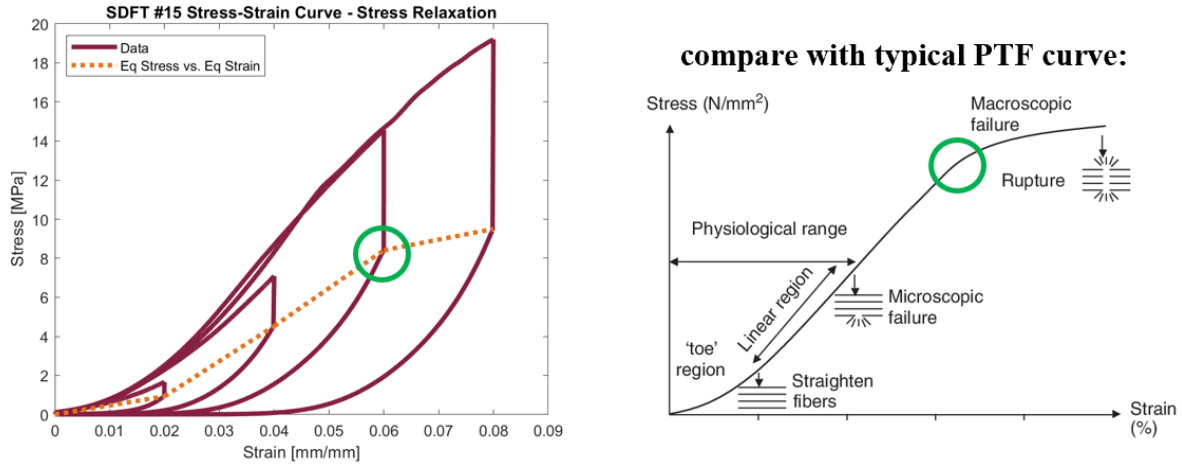
Figure 4-1: A reproduction of Figure 3-1 compared to a typical monotonic pull-to-failure curve with representations of fiber behavior during various points of the curve, adapted from Wang [25].

One challenge associated with collecting mechanical failure data from biological tissue is the gripping of the specimen. Applying sufficient gripping force while simultaneously avoiding crushing the tendon in the process is notably difficult, and often results in significant variation while conducting pull-to-failure tests without the use of extra measures such as freezer gripping, sample sectioning, or bone fragment potting [73]. Flexor tendons have extremely low external friction and high tensile strength, requiring creative methods to achieve sufficient gripping force without damaging the sample [74]. However, the entire tissue had to remain submerged in saline during this test for US imaging purposes during the course of the mechanical tests, ruling out the use of freezer grips. A series of progressive subfailure strain holds still allowed for the mechanical characterization of the SDFT, circumventing the unfrozen grips limitation since smaller loads were still sufficient to generate damage and extract E_{eq}. The similarities shown between E_{eq} and the modulus in a typical pull-to-failure indicate the utility of subfailure testing for tissue characterization.

D_s as measured at preload (2 N) following a recovery period differentiated the 6% and 8% strain levels. This parameter quantifies the ability of the tendon to recover its original length following a strain hold. Although the stress relaxation behavior of tendons has been well-established, less is known about the recovery from stress relaxation [3]. Regardless of the exact microscale processes that enact this change, excessive tendon laxity has been identified as a risk factor for lower limb injury [75]. This lends credence to the connection between laxity and damage, established by Provenzano et al [32]. If the general population is more likely to experience tendinopathy from having lax tendons, it can be concluded that a process that increases the laxity

40

of a tendon is damaging it. This damage is evidently occurring in the SDFT samples during the 6% strain level, agreeing with threshold identified by E_{eq}.

No significant differences were observed in %Rlx across the four strain levels. Although it is expected that stress relaxation would be reduced in damaged tendons, porcine SDFT has also been shown to exhibit a higher degree of relaxation at higher strain levels [31, 35]. This potentially confounding factor of strain could account for the flat distribution of relaxation percentages.

4.1.2 Protocol 2 – Damage Ramp

Contrary to the initial hypothesis and the results of the stress relaxation tests, E_{eq} rose after the damage ramp at 10% strain. This result has been observed previously in avian flexor tendons, where a short, subfailure strain ramp did not affect the properties—including elastic modulus—measured during a subsequent pull-to-failure [76]. On the other hand, when adequate rest was provided after the damage ramp (20 vs. 5 minutes) and a stress relaxation was used to evaluate properties instead of a pull-to-failure, properties were found to be reduced significantly after a high-strain, subfailure ramp in a porcine SDFT, as expected [33]. Both of these adjustments in the porcine study corrected for potential viscous effects that could have confounded the results of the avian study. One potential explanation for the result in the present study is that because the 2% strain was measured using the length at preload as L_0, the laxed tendon was pulled to a longer absolute length after the damage ramp. This is closer to a measurement of true strain, ε, in which the gauge length, L_0, is constantly refreshed and strain is calculated based on the summed incremental additions to the overall length [77].

$$\varepsilon = \int_{L_0}^{L} \frac{dL}{L} = \ln \frac{L}{L_0}$$

Equation 11

In contrast, engineering strain is based on the net change in length from the original length, which in this case would be the length at preload prior to the damage ramp. After adjusting E_{eq} for engineering strain assumptions, it shows a decrease after the damage ramp.

During the damage ramp, the tissue did exhibit a large degree of hysteresis, returning approximately half of the energy delivered while straining to 10%. The damping capacity of a tendon can indicate its damage state, as accumulation of subfailure fatigue can cause a loss of hysteresis [78]. Since this was only a single ramp, no comparisons can be drawn to evaluate the

damage state based on hysteresis loss, but the large value of hysteresis does indicate that following the initial 2% stress relaxation, the tendon remained structurally sound. The stress-strain curve for the damage ramp does indicate evidence of post-yield behavior, with 6 of the 8 specimens experiencing peak instantaneous modulus measurements prior to reaching 10% strain. On average, this yielding occurred in a tight window around a mean of 5.29% strain, despite large variation in yield stress from the different samples. This measurement aligns with the results of the progressive stress relaxation, which identified a reduction in tendon mechanical properties following the 6% strain level, as well as previous literature [25, 32]. Taken together, the mechanical analysis from the damage ramp itself indicates that the initial section of progressive stress relaxation testing done in this experiment was successful in identifying not just a strain level that would not incur significant damage, but also one that would. As expected, the yield stress, yield strain, and modulus measured during the damage ramp were all significantly higher than those measured during the post-stress relaxation residual strength pull-to-failure. However, this may have been influenced by the increased strain rate during the damage ramp compared to the pull-to-failure, which has been shown to produce higher instantaneous stresses in viscoelastic materials [27].

In agreement with the progressive stress relaxation testing, D_s was also increased following the damage ramp. After the 10% ramp, the mean laxity in the specimen was similar to that found after the 6% strain level, although much less than that found after the 8% strain level. This suggests that tendon laxity is influenced by load duration as well as magnitude. Translating this conclusion to the clinical setting, the damage sustained by a tendon from a single injury event could be considered comparable to long-term overuse in terms of resulting tendon laxity.

The percentage of stress relaxed in the tendon at the same 2% strain level was significantly decreased following a damage ramp, in agreement with the previous porcine SDFT mechanics study [33]. This was perhaps the strongest indicator in this set of tests that tendon damage had taken place during the acute ramp. By repeating the same strain level, the confounding effect of higher strain on %Rlx during the progressive stress relaxation was dissipated.

4.2   Sonographic Analysis

4.2.1   Protocol 1 & 2 – Progressive Stress Relaxation & Damage Ramp

Across both methodologies, texture features associated with non-uniformity, entropy, and coarseness increased significantly between tendons that had experienced damage. The progressive

42

stress relaxation tests alone identified significantly different energy and correlation outcomes while the damage ramp alone identified significantly different variance parameters. The directions of these observed changes are listed in Table 7, along with a proposed explanation based on the formulation of the parameters.

Table 7: Observed changes across texture parameter types after damage had occurred.

General Parameter Type	Direction of Δ with damage	Reasoning
Variance	↓	Thinner histogram
Energy (ASM)	↑	Fewer consistent patterns
Entropy	↓	More homogeneous
Correlation	↓	Less granularity
Non-Uniformity	↑	Less repetitive structure
Coarseness	↓	Smoother texture from fewer visible fibers

No significant differences were found between mean echogenicity at any damage level. As previous *ex vivo* studies have shown, mean echogenicity may encompass too many confounding factors to effectively draw conclusions from its value, with Schmidt and Duenwald et al. producing conflicting results as to the direction of change of mean echogenicity with damage [64, 65]. In contrast, *in vivo* studies consistently see significant reductions in mean echogenicity [52, 54, 60], suggesting that the factors involved in darkening tendon sonographs may be biologic in nature, rather than mechanical. Collinger et al. extended their analysis to include seven other first order and GLCM statistics in a quantitative analysis of shoulder tendon injuries, and found that the second order parameters were more sensitive to tendon pathology [54]. Replicating this analysis with patients suffering from Achilles tendinopathy, Nadeau et al. found that second order parameters had better reliability in distinguishing between symptomatic and asymptomatic individuals than first order parameters, indicating that second order parameters were more robust to different experimental protocols [53]. Similar results were seen in the patellar tendon as well [60]. Analyzing even more than two pixels at once seems to further improve these outcomes as higher order parameters made up the majority of those that were capable of distinguishing between damage levels in this study. Since there are many factors that affect the consistency of images acquired by ultrasound, reliably consistent measurements are at a premium. This study has demonstrated that higher order parameters are sensitive to changes in tendon damage state, and the robustness of non-uniformity, entropy, and coarseness to multiple experimental protocols

establishes promising candidates for tendinopathy diagnosis that may be uniquely resilient to factors such as US machine and probe operation. Future *in vivo* studies should assess both the sensitivity and reliability of higher order parameters in correctly diagnosing tendinopathy.

The gray-level co-occurrence matrix (GLCM) has been studied more extensively in muscle than tendon. GLCM energy (angular second moment), entropy, and correlation differed significantly between amyotrophic lateral sclerosis (ALS) patients and healthy controls [57], and could also effectively track disease progression over time [56]. In these studies, muscular atrophy caused by the progression of this neurodegenerative disease caused an increase in entropy, and a decrease in energy and correlation. These are apparently opposite results to those generated from this study, but it was noted that amyotrophic muscle exhibits higher levels of granularity due to fibrosis, as opposed to lower expected granularity from injured tendon. This emphasizes the difference in radiomic parameter evaluation between different tissue types. Demographic and performance effects in healthy individuals were also observed across GLCM parameters, with GLCM entropy and energy found to differ significantly with age and maximum torque output [79], as well as sex [49]. Microscopy-based studies of GLCM in collagen fiber arrangement also highlighted these same parameters of energy, entropy, and correlation in distinguishing the orderliness of fibers [50, 80]. Again, it is an encouraging result that across tissue types, testing protocols, and disease states, these three biomarkers are in consistent agreement with pathological status. There were no significant differences identified between GLCM parameters during the damage ramp tests in this study.

4.3   Limitations

Although it facilitates ultrasound image clarity for the purposes of texture analysis, one trade-off of using *ex vivo* tendons as opposed to living tissue in this study was that it was not possible to examine the cellular response to mechanical stimulus, which may have increased damage resistance [81]. Another consequence of *ex vivo* testing is that the longevity of the testing period for Protocol 1 may have contributed to tissue degradation, as tendons were submerged for approximately 4 hours. This duration was necessary to ensure all tendons tested reached equilibrium and were given a reasonable period of time to recover between strain applications. Measures were taken to limit tendon breakdown, such as using a fresh 10 liters of saline for each test. Encouragingly, similar results were observed for the mechanical and textural parameters

between the shorter Protocol 2 and the lengthier Protocol 1, indicating a potentially minimal effect of tendon degeneration on experimental outcomes.

A relatively small sample size of 14 tendons were used in this project due to the lengthy nature of testing and because many of the measures were made within subjects, resulting in a large number of total images, despite the few tendons used. Although it is expected that the texture results for this tendon will be broadly applicable to most energy-storing tendons, it is noted that in racehorses, only SDFTs in forelimbs experienced injury [16], while only hindlimb SDFTs were examined in this study.

Chapter 5: Conclusion

Radiomic analysis of ultrasound images is a promising source of biomarkers to distinguish uninjured from injured tendon in the context of tendinopathy. In what is, to our knowledge, the first study to apply texture analysis to tendons imaged and loaded *ex vivo*, parameters regarding the orderliness and uniformity of the tendon were found to differ significantly depending on the amount of damaging loads the tendon had received. The precise control exerted in this study over tendon damage state and imaging confounders usually associated with ultrasound imaging supports the translation of these outcomes towards a clinical setting. Specifically, a clinician could use these radiomic parameters to support their conclusions made from ultrasound in evaluating the severity of a tendinopathy case. An athletic department or sporting organization that may have a large proportion of at-risk individuals could go a step further and create profiles for individual athletes from regular ultrasound screenings and analyses, evaluating changes over time in key tendon radiomic parameters as an early indicator of imminent injury. The two methodologies of dosing damage produced some comparable but also many distinct results in terms of the textural properties observed. This could indicate that a radiomic analysis may differ by the mechanism of tendon injury. For example, a tendon strain resulting from sudden movement similar to the damage ramp may present clinically with lower variance compared to pre-injury scans, while an overuse tendinopathy modeled by the progressive stress relaxation might present with lower entropy and correlation. Further study is warranted to verify if higher order texture parameters could show similarly sharp diagnostic prowess for *in vivo* tendinopathy.

References

1.	Docheva, D., et al., *Biologics for tendon repair.* Advanced Drug Delivery Reviews, 2015. **84**: p. 222-239.
2.	Screen, H., et al., *Extrafibrillar diffusion and intrafibrillar swelling at the nanoscale are associated with stress relaxation in the soft collagenous matrix tissue of tendons.* Soft Matter, 2011. **7**(23): p. 11243-11251.
3.	Legerlotz, K., G.P. Riley, and H.R.C. Screen, *GAG depletion increases the stress-relaxation response of tendon fascicles, but does not influence recovery.* Acta Biomaterialia, 2013. **9**(6): p. 6860-6866.
4.	Cribb, A.M. and J.E. Scott, *Tendon response to tensile stress: an ultrastructural investigation of collagen:proteoglycan interactions in stressed tendon.* J Anat, 1995. **187 (Pt 2)**(Pt 2): p. 423-8.
5.	Chuen, F.S., et al., *Immunohistochemical Characterization of Cells in Adult Human Patellar Tendons.* Journal of Histochemistry & Cytochemistry, 2004. **52**(9): p. 1151-1157.
6.	Maffulli, N., *Overuse tendon conditions: Time to change a confusing terminology.* Arthroscopy: The Journal of Arthroscopic & Related Surgery, 1998. **14**(8): p. 840-843.
7.	Sobhani, S., et al., *Epidemiology of ankle and foot overuse injuries in sports: A systematic review.* Scandinavian Journal of Medicine & Science in Sports, 2013. **23**(6): p. 669-686.
8.	Janssen, I., et al., *Investigating Achilles and patellar tendinopathy prevalence in elite athletics.* Research in Sports Medicine, 2018. **26**(1): p. 1-12.
9.	de Jonge, S., et al., *Incidence of midportion Achilles tendinopathy in the general population.* British Journal of Sports Medicine, 2011. **45**(13): p. 1026.
10.	Fredberg, U. and L. Bolvig, *Significance of Ultrasonographically Detected Asymptomatic Tendinosis in the Patellar and Achilles Tendons of Elite Soccer Players: A Longitudinal Study.* The American Journal of Sports Medicine, 2002. **30**(4): p. 488-491.
11.	Fredberg, U. and K. Stengaard-Pedersen, *Chronic tendinopathy tissue pathology, pain mechanisms, and etiology with a special focus on inflammation.* Scandinavian Journal of Medicine & Science in Sports, 2008. **18**(1): p. 3-15.
12.	McAuliffe, S., et al., *Can ultrasound imaging predict the development of Achilles and patellar tendinopathy? A systematic review and meta-analysis.* British Journal of Sports Medicine, 2016. **50**(24): p. 1516.
13.	Kannus, P. and L. Józsa, *Histopathological changes preceding spontaneous rupture of a tendon. A controlled study of 891 patients.* J Bone Joint Surg Am, 1991. **73**(10): p. 1507-25.
14.	Lichtwark, G.A. and A.M. Wilson, *In vivo mechanical properties of the human Achilles tendon during one-legged hopping.* J Exp Biol, 2005. **208**(Pt 24): p. 4715-25.
15.	Herrick, W.C., H.B. Kingsbury, and D.Y.S. Lou, *A study of the normal range of strain, strain rate, and stiffness of tendon.* Journal of Biomedical Materials Research, 1978. **12**(6): p. 877-894.
16.	Ely, E.R., et al., *Descriptive epidemiology of fracture, tendon and suspensory ligament injuries in National Hunt racehorses in training.* Equine Vet J, 2009. **41**(4): p. 372-8.
17.	Brown, A., *Dissection of Pelvic Limb*, in *Dissection Lab Guide for Ungulate Anatomy*. University of Minnesota.

18.	Barfod, K., *Achilles tendon rupture; Assessment of nonoperative treatment.* Danish medical journal, 2014. **61**: p. B4837.

19.	Zhou, X., D. Yu, and O. Barrera, *Chapter Three - Mechanics constitutive models for viscoelastic solid materials: Development and a critical review*, in *Advances in Applied Mechanics*, S.P.A. Bordas, Editor. 2023, Elsevier. p. 189-321.

20.	Lee, A.H., et al., *Investigating mechanisms of tendon damage by measuring multi-scale recovery following tensile loading.* Acta Biomater, 2017. **57**: p. 363-372.

21.	Kelc, R., K. Matevz, and V. Matjaz, *The Physiology of Sports Injuries and Repair Processes*, in *Current Issues in Sports and Exercise Medicine*, M.J. Hamlin and N. Draper, Editors. 2013, IntechOpen: Rijeka.

22.	Lake, S.P., et al., *Guidelines for ex vivo mechanical testing of tendon.* J Orthop Res, 2023. **41**(10): p. 2105-2113.

23.	Screen, H.R.C., *Investigating load relaxation mechanics in tendon.* Journal of the Mechanical Behavior of Biomedical Materials, 2008. **1**(1): p. 51-58.

24.	Screen, H.R., S. Toorani, and J.C. Shelton, *Microstructural stress relaxation mechanics in functionally different tendons.* Med Eng Phys, 2013. **35**(1): p. 96-102.

25.	Wang, J., *Mechanobiology of tendon—Review.* Journal of biomechanics, 2006. **39**: p. 1563-82.

26.	Peloquin, J.M., M.H. Santare, and D.M. Elliott, *Advances in Quantification of Meniscus Tensile Mechanics Including Nonlinearity, Yield, and Failure.* J Biomech Eng, 2016. **138**(2): p. 021002.

27.	Lynch, H.A., et al., *Effect of fiber orientation and strain rate on the nonlinear uniaxial tensile material properties of tendon.* J Biomech Eng, 2003. **125**(5): p. 726-31.

28.	Grant, T.M., et al., *The Mechanical, Structural, and Compositional Changes of Tendon Exposed to Elastase.* Annals of Biomedical Engineering, 2015. **43**(10): p. 2477-2486.

29.	Sasajima, S., et al., *Effect of relaxation time on hysteresis of human tendon in vivo.* J Musculoskelet Neuronal Interact, 2023. **23**(1): p. 84-89.

30.	Graf, B.K., et al., *Effect of preconditioning on the viscoelastic response of primate patellar tendon.* Arthroscopy: The Journal of Arthroscopic & Related Surgery, 1994. **10**(1): p. 90-96.

31.	Duenwald, S.E., R. Vanderby, Jr., and R.S. Lakes, *Viscoelastic relaxation and recovery of tendon.* Ann Biomed Eng, 2009. **37**(6): p. 1131-40.

32.	Provenzano, P.P., et al., *Subfailure damage in ligament: a structural and cellular evaluation.* J Appl Physiol (1985), 2002. **92**(1): p. 362-71.

33.	Duenwald-Kuehl, S., et al., *Damage mechanics of porcine flexor tendon: mechanical evaluation and modeling.* Ann Biomed Eng, 2012. **40**(8): p. 1692-707.

34.	Olvera, D., A. Daly, and D.J. Kelly, *Mechanical Testing of Cartilage Constructs*, in *Cartilage Tissue Engineering: Methods and Protocols*, P.M. Doran, Editor. 2015, Springer New York: New York, NY. p. 279-287.

35.	Ciarletta, P., et al., *A novel microstructural approach in tendon viscoelastic modelling at the fibrillar level.* Journal of Biomechanics, 2006. **39**(11): p. 2034-2042.

36.	Lawrence, J.P., *Physics and instrumentation of ultrasound.* Critical Care Medicine, 2007. **35**(8): p. S314-S322.

37.	Pillen, S. and N. and van Alfen, *Skeletal muscle ultrasound.* Neurological Research, 2011. **33**(10): p. 1016-1024.

38.   Mitchell, M., *Assessment of Patellar Tendons Over the Course of a Collegiate Men's and Women's Basketball Season Using Gray-Scale Ultrasound and Shear-Wave Elastography*. 2020: AOASM Annual Conference.

39.   Warden, S.J., et al., *Comparative Accuracy of Magnetic Resonance Imaging and Ultrasonography in Confirming Clinically Diagnosed Patellar Tendinopathy.* The American Journal of Sports Medicine, 2007. **35**(3): p. 427-436.

40.   Parker, L., et al., *Musculoskeletal imaging: medicare use, costs, and potential for cost substitution.* J Am Coll Radiol, 2008. **5**(3): p. 182-8.

41.   Weinreb, J.H., et al., *Tendon structure, disease, and imaging.* Muscles Ligaments Tendons J, 2014. **4**(1): p. 66-73.

42.   Paantjens, M., et al., *The interrater reliability of ultrasonography for Achilles tendon structure.* J Ultrason, 2020. **20**(80): p. e6-e11.

43.   O'Connor, P.J., et al., *Ultrasound assessment of tendons in asymptomatic volunteers: a study of reproducibility.* European Radiology, 2004. **14**(11): p. 1968-1973.

44.   Paris, M.T. and M. Mourtzakis, *Muscle Composition Analysis of Ultrasound Images: A Narrative Review of Texture Analysis.* Ultrasound Med Biol, 2021. **47**(4): p. 880-895.

45.   Bharati, M.H., J.J. Liu, and J.F. MacGregor, *Image texture analysis: methods and comparisons.* Chemometrics and Intelligent Laboratory Systems, 2004. **72**(1): p. 57-71.

46.   Castellano, G., et al., *Texture analysis of medical images.* Clin Radiol, 2004. **59**(12): p. 1061-9.

47.   Aggarwal, N. and R. Agrawal, *First and Second Order Statistics Features for Classification of Magnetic Resonance Brain Images.* Journal of Signal and Information Processing, 2012. **03**.

48.   Haralick, R.M., K. Shanmugam, and I. Dinstein, *Textural Features for Image Classification.* IEEE Transactions on Systems, Man, and Cybernetics, 1973. **SMC-3**(6): p. 610-621.

49.   Molinari, F., et al., *Advances in Quantitative Muscle Ultrasonography Using Texture Analysis of Ultrasound Images.* Ultrasound in Medicine & Biology, 2015. **41**(9): p. 2520-2532.

50.   Hu, W., et al., *Characterization of collagen fibers by means of texture analysis of second harmonic generation images using orientation-dependent gray level co-occurrence matrix method.* Journal of Biomedical Optics, 2012. **17**(2): p. 026007.

51.   Kozar, Z.C., *Quantitative Analysis Of Sonographic Images Of Patellar Tendons In Collegiate Women's Basketball Players Using Shear Wave Elastography Texture Analysis*, in *Orthopaedic Research Society*. 2021. p. 1632L.

52.   Lalumiere, M., et al., *To What Extent Do Musculoskeletal Ultrasound Biomarkers Relate to Pain, Flexibility, Strength, and Function in Individuals With Chronic Symptomatic Achilles Tendinopathy?* Front Rehabil Sci, 2021. **2**: p. 726313.

53.   Nadeau, M.J., et al., *Quantitative ultrasound imaging of Achilles tendon integrity in symptomatic and asymptomatic individuals: reliability and minimal detectable change.* J Foot Ankle Res, 2016. **9**: p. 30.

54.   Collinger, J.L., et al., *Validation of grayscale-based quantitative ultrasound in manual wheelchair users: relationship to established clinical measures of shoulder pathology.* Am J Phys Med Rehabil, 2010. **89**(5): p. 390-400.

55.   Zwanenburg, A., et al., *Image biomarker standardisation initiative.* arXiv preprint arXiv:1612.07003, 2016.

56.	Martínez-Payá, J.J., et al., *Monitoring Progression of Amyotrophic Lateral Sclerosis Using Ultrasound Morpho-Textural Muscle Biomarkers: A Pilot Study.* Ultrasound in Medicine & Biology, 2018. **44**(1): p. 102-109.

57.	Martínez-Payá, J.J., et al., *Quantitative Muscle Ultrasonography Using Textural Analysis in Amyotrophic Lateral Sclerosis.* Ultrason Imaging, 2017. **39**(6): p. 357-368.

58.	Amadasun, M. and R. King, *Textural features corresponding to textural properties.* IEEE Transactions on Systems, Man, and Cybernetics, 1989. **19**(5): p. 1264-1274.

59.	Galloway, M.M., *Texture analysis using gray level run lengths.* Computer Graphics and Image Processing, 1975. **4**(2): p. 172-179.

60.	Crimmins, S., *Quantitative Texture and Blob Analyses on Patellar Tendon Sonographic Images of Collegiate Basketball Athletes*, in *Biomedical Engineering*. 2023, Virginia Tech.

61.	Sun, C. and W.G. Wee, *Neighboring gray level dependence matrix for texture classification.* Computer Vision, Graphics, and Image Processing, 1983. **23**(3): p. 341-352.

62.	Backhaus, M., et al., *Guidelines for musculoskeletal ultrasound in rheumatology.* Ann Rheum Dis, 2001. **60**(7): p. 641-9.

63.	Duenwald, S., et al., *Ultrasound echo is related to stress and strain in tendon.* J Biomech, 2011. **44**(3): p. 424-9.

64.	Schmidt, E.C., et al., *Ultrasound echogenicity is associated with fatigue-induced failure in a cadaveric Achilles tendon model.* J Biomech, 2020. **105**: p. 109784.

65.	Duenwald-Kuehl, S., R. Lakes, and R. Vanderby, Jr., *Strain-induced damage reduces echo intensity changes in tendon during loading.* J Biomech, 2012. **45**(9): p. 1607-11.

66.	Riggin, C.N., et al., *Analysis of collagen organization in mouse achilles tendon using high-frequency ultrasound imaging.* J Biomech Eng, 2014. **136**(2): p. 021029.

67.	Casarotto, R.A., et al., *Coupling agents in therapeutic ultrasound: acoustic and thermal behavior.* Arch Phys Med Rehabil, 2004. **85**(1): p. 162-5.

68.	Ji, L., J. Piper, and J.-Y. Tang, *Erosion and dilation of binary images by arbitrary structuring elements using interval coding.* Pattern Recognition Letters, 1989. **9**(3): p. 201-209.

69.	Zijdenbos, A.P., et al., *Morphometric analysis of white matter lesions in MR images: method and validation.* IEEE Transactions on Medical Imaging, 1994. **13**(4): p. 716-724.

70.	van Griethuysen, J.J.M., et al., *Computational Radiomics System to Decode the Radiographic Phenotype.* Cancer Res, 2017. **77**(21): p. e104-e107.

71.	Witt, J.C., *Equilibrium Testing of Rat Tail Tendon: An Analysis of the Viscoelastic Properties of Collagen Under Different Strain Points*, in *Biology & Biomedical Engineering*. 2016, Rose-Hulman Institute of Technology.

72.	Mow, V., et al., *Mow VC, Kuei SC, Lai WM, Armstrong CG. Biphasic creep and stress relaxation of articular cartilage in compression: Theory and experiments. J Biomech Eng 102: 73-84.* Journal of biomechanical engineering, 1980. **102**: p. 73-84.

73.	Wale, M.E., et al., *Applying ASTM Standards to Tensile Tests of Musculoskeletal Soft Tissue: Methods to Reduce Grip Failures and Promote Reproducibility.* J Biomech Eng, 2021. **143**(1).

74.	Matthews, G.L., K.G. Keegan, and H.L. Graham, *Effects of tendon grip technique (frozen versus unfrozen) on in vitro surface strain measurements of the equine deep digital flexor tendon.* Am J Vet Res, 1996. **57**(1): p. 111-5.

75.   Tingle, A., et al., *The links between Generalized Joint Laxity and the incidence, prevalence and severity of limb injuries related to physical exercise: a systematic literature review.* Physical Therapy Reviews, 2018. **23**(4-5): p. 259-272.

76.   Devkota, A.C. and P.S. Weinhold, *Mechanical response of tendon subsequent to ramp loading to varying strain limits.* Clinical Biomechanics, 2003. **18**(10): p. 969-974.

77.   Nisbett, K. and R. Budynas, *Shigley's Mechanical Engineering Design, 10th Edition.* 2015.

78.   Andarawis-Puri, N., et al., *The relationships between cyclic fatigue loading, changes in initial mechanical properties, and the in vivo temporal mechanical response of the rat patellar tendon.* J Biomech, 2012. **45**(1): p. 59-65.

79.   Watanabe, T., et al., *Quantitative Sonographic Assessment of the Quadriceps Femoris Muscle in Healthy Japanese Adults.* Journal of Ultrasound in Medicine, 2017. **36**(7): p. 1383-1395.

80.   Cicchi, R., et al., *Scoring of collagen organization in healthy and diseased human dermis by multiphoton microscopy.* Journal of Biophotonics, 2010. **3**(1-2): p. 34-43.

81.   Kjaer, M., *Role of extracellular matrix in adaptation of tendon and skeletal muscle to mechanical loading.* Physiol Rev, 2004. **84**(2): p. 649-98.

Appendix A – Dissection Protocol

Materials

- Size 10, 11, and 24 blades with scalpel handles
- Forceps
- Clamps
- Flat tool
- Absorbent pad
- Cutting board
- Autoclave bag
- Saline

Stage 1: Preparation

1. Remove the specimen from the freezer still in the bag and place in a water bath.
2. Wrap any portion of the specimen that is not submerged in saline-soaked gauze.
3. Wait 12-48 hours depending on specimen size.

Stage 2: Day-of Setup and Extra Tissue Removal

4. Place absorbent pad, cutting board, and autoclave bag in fume hood.
5. Remove the specimen from the water bath and place it on the cutting board.

6. Manipulate the leg to locate the patellar and SDFT tendons.

Stage 3: Superficial Digital Flexor Tendon (SDFT) Removal

7. Make skin-deep incisions on the medial and lateral sides of the hip and unfold the skin from the anterior side of the leg, using the forceps to grip the skin while cutting away from the quadriceps muscle and knee.

8. Manipulate foot to raise Achilles and superficial digital flexor tendons against the skin surface and palpate to locate the entire tendon width.

9. Unfold the skin from the anterior side of the leg down to the ankle, using the forceps to grip the skin while cutting away from the muscle tissue around the tibia.

10. Remove excess muscle in the hip and upper thigh areas.

11. Separate the interior (those attached to the tibia) and exterior muscular structures (those attached to the Achilles and SDFT) in the calf. The exterior muscular structures insert at the posterior of the knee as shown below at left. Cutting the insertion should allow the tibia to move freely between the 90 and 180 degree positions now that it is no longer constrained by the Achilles tendon shown below at right.

12. Cut any remaining fascial connective tissue between the exterior and interior muscle structures.
13. Cut the deep digital flexor just above the ankle to further release the tibial range of motion.
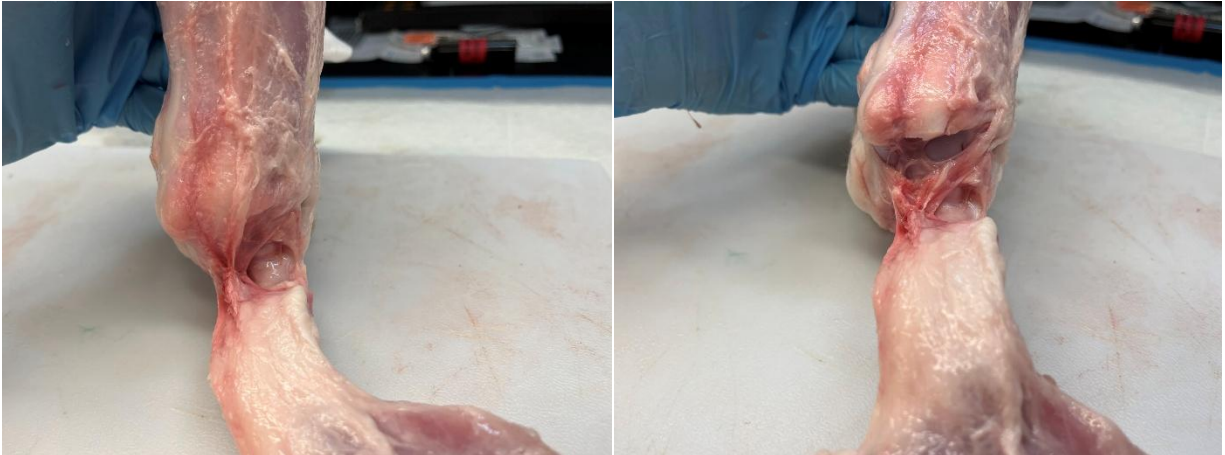
14. Unfold the skin from the posterior side of the leg, using the forceps to grip the skin while carefully cutting the fat away from the tissue around the tendon.

15. With the skin around the heel removed and the calf muscles separated from the tibia, the strategy for the next couple of steps is to expose the insertion point of the AT. There is a significant amount of adipose tissue in this region. To remove it, grasp and pull up with forceps and make cuts on the tissue parallel to the tendon. Although the adipose tissue resembles tendon, mistakes in this region attacking the top of the calcaneus would hit the AT first before the SDFT.

16. At this point it should become possible to separate the muscular structures associated with the AT from those associated with the SDFT manually. It may be necessary to remove a thin fascial layer covering the two muscles first.

17. Tilting the leg so the toes are down and the heel is up makes the AT insertion site more obvious. Cut the AT at its insertion site. The SDFT does not have any insertion to the calcaneus and can instead be identified by the relatively hard plate that wraps around the outside of the heel. In the photo below, the severed AT is gripped by the forceps and the SDFT spans the gap.

18. Insert the flat tool into the gap between the heel plate and the Achilles from the distal end to facilitate the separation of the two tendons. There will be some resistance from connective tissue in the gap, but the flat tool is unable to puncture tendons, so it is safe to force the tool through.
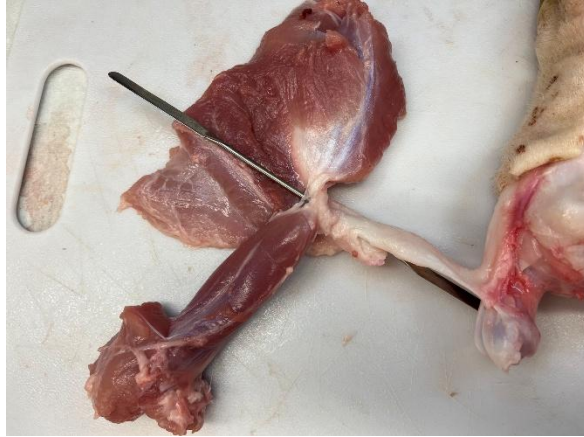
19. The most difficult step is the midsubstance severance of the AT. This is because the AT and SDFT essentially cross over one another in a region of dense adipose tissue. Taking your time and using the flat tool and forceps to elevate the AT, gradually split the tendon longitudinally.
20. Cut the connective tissue between the split AT and the SDFT on both sides and dispose of AT and its associated muscle body. The result is shown below.

21. Make medial and lateral cuts along the foot and remove any remaining skin from the volar aspect using the same folding back and cutting technique as before.
22. Angling the blade towards the bone in the foot and lifting the SDFT, cut the tendon away. Using this technique, it is likely that some of the deep digital flexor tendon will be cut away as well, which will need to be removed later.
23. Sever the tendon insertion around the region where it splits to feed into the toes.
24. Shave and scrape the muscle off of the SDFT using the flat tool and the dull back side of the scalpels, being careful not to pull on the tendon excessively.

25. Place the SDFT in a petri dish containing saline solution or in saline soaked gauze and a labeled bag.

Stage 4: Clean up

26. Since the remaining specimen may be used by other students in the lab, use another labeled bag to store it in the freezer, making sure to cover as much of the remaining sample as possible in skin and saline-soaked gauze to shield it from outside effects.
27. Put the bagged tendon samples in the freezer for storage.
28. Carefully remove scalpel blades from their handles and place them in biological sharps disposal.
29. Wash the cutting board, scalpel handles, forceps, clamps, and flat tool and put them on the drying rack above the sink.
30. Dispose of any leftover tissue and the absorbent pad in the autoclave bag, then tie it off and place it in the freezer.
31. Wipe down the inside of the fume hood and any other work surfaces with ethanol.
32. Deglove and wash hands and forearms thoroughly.

Appendix B – MTS Test Protocol

Phase 1 – Sample Preparation

1. Thaw tendon
   a. Remove bagged tendon from freezer and place in a room temperature water bath
   b. Leave for 20 minutes
2. If necessary, use a size 11 scalpel to scrape and remove any remaining muscle tissue from the proximal end of the specimen
3. Measure the tendon width 3 times in the medial portion (where the x-section is smallest) and calculate the average width
4. Measure the tendon thickness 3 times at approximately the same location as the width measurement and calculate the average thickness
5. Calculate the tendon cross-sectional area using the ellipse formula, $A = \frac{\pi}{4}wt$

Phase 2a – Testing Preparation

6. Make 10 L of saline (9 g of NaCl/1 L H20 -> 90 g of NaCl/10 L H20)
7. Fix the platen to the bottom plate using a ¼-20 countersunk screw
8. Fix the bottom plate in place using the four t-nuts, aligning the platen with the MTS crosshead.
9. Place the PCA tank on the base plate such that the platen goes through the PVC-lined hole in the center, securing the tank in place with side brackets and 8 8-32 - 1" socket head screws.

10. Apply the slip joint fitting around the platen and screw on the large plastic nut to apply a compression seal to the PCA tank. (optional: add orange o-ring before the plastic nut for decreased leakage)

Phase 2b – Gripping

11. Screw the bottom grip-mount (size ¼-20) onto the threaded rod in the platen at the base of the MTS.
12. Screw the M6 threaded rod into the MTS insert loosely, then insert it into the load cell and pin in place. The pin is held in place by the M6 rod (see step 14 if pin remains loose in load cell/insert interface.
13. Screw two jam nuts onto the M6 rod.
14. Screw the top grip-mount (size M6) onto the M6 threaded rod until reasonably tight. Tighten one jam nut onto the top of the grip-mount. If the pin at the load cell/insert interface is still loose, it should be possible to tighten it by manually turning the top grip-mount since its translation up the M6 threaded rod is now blocked by the jam nut. Hold the jam nut against the rotation of the grip-mount using a wrench if necessary. This may be less effective with softer resin grip-mounts.
15. Tighten one jam nut on insert.
16. Once the pin is secured, loosen the jam nut on the top grip-mount and rotate the top grip-mount to be aligned with the bottom grip-mount. Tighten the jam nut on the top grip-mount again.
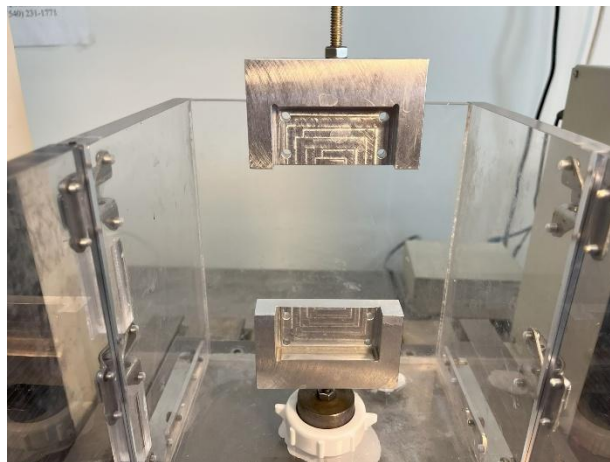
17. Grip tendon

a. Place the threaded side of the grips into the sliding guide.
   b. Place the tendon ends on each of the threaded grip plates.
   c. Align the grips so that the exposed region of the tendon is equivalent to the previously calculated gauge length. Use calipers to measure this distance
   d. Place the non-threaded side of the flat sandpaper grip on top of their respective sides.
   e. Insert 4 8-32 socket head screws into each of the grips and tighten, making sure to close the grips evenly. Measure the final grip to grip length to ensure that it is equal to the calculated gage length
18. Mount grips in grip-mounts using 8 8-32 kep nuts. If necessary, turn on the MTS and move the crosshead into an appropriate position to maintain slack on the tendon while mounting grips. Turn MTS off once completed.

Phase 2c – Imaging Setup

19. Align the PCA tank extender with the PCA tank and latch into place.
20. Place the ultrasound probe holder on the tank and insert the probe into the holder.

21. Arrange the probe so that it is aligned with the tendon and close to the tendon without touching the grips. Align the bottom of the probe with the top of the bottom grips. Tighten knobs on probe holder joints to secure the probe in a stationary position.
22. Turn on the Aixplorer clinical ultrasound machine.
23. Log into the lab computer and launch TestworksElite (TWE).

Phase 3a – Preconditioning

24. On TWE select the preconditioning template labeled SLH_Preconditioning. Turn on the MTS and connect to the Controller by navigating to Controller > Connect on the toolbar.
25. Place the tendon in slack and zero the load measurement in TWE. Measure the length of the tendon at this point using calipers and write it down as the Grips Gage Length.

26. Fill the tank with the premade saline from Phase 1. Ensure a clear image appears on the US machine screen once the fluid settles.

27. Zero the load measurement in TWE (the saline causes a buoyant effect in the fixtures and specimen).

28. Start the program. Input measured Width, Thickness, and Grip Gage Length.
    a. The load will increase to **2 N** and hold the resulting extension for **3'** to overshoot the desired preload value of **1 N**. Write down this extension as displayed as Preload Additional Length. Add Grips Gage Length to Preload Additional Length to get Adjusted Gage Length.
    b. At the end of **3'**, the program will do part (a) automatically, measuring the net extension required to achieve preload and adding it to the initial Gage Length. Extension will then reset to zero.
    c. The program will go directly into preconditioning. This program will cycle the tendon from **2 N** to **4 N** at **0.5 mm/s** for **20 cycles**.
    d. When prompted, click "Yes" on the "Return to zero?" window

29. After the preconditioning program has concluded, allow the sample to recover at the Grips Gage Length (slack) for **5'**. Crosshead and Extension should both read zeroes at this point.

30. Save the test file and raw data. Proceed to either Phase 3b or 3c.

Phase 3b – Progressive Stress Relaxation

31. On TWE select the stress relaxation template labeled SLH_SR.

32. Place the tendon in complete slack and zero the load measurement in TWE.

33. Increase the load on the hand controller to the point where the load cell registers a reading greater than **0.05 N**. Measure this length using calipers and write it down as the Grips Gage Length.

34. Input **2% strain** level in the MTS Procedure.

35. Start the program. Input measured Width, Thickness, and Grips Gage Length. During preloading, take a BMode and SWE image on the US machine.
    a. The load will increase to **2 N** and hold the resulting extension for **3'** to overshoot the desired preload value of **1 N**. Write down this extension as displayed as Additional Length. Add Grips Gage Length to Additional Length to get Adjusted Gage Length.
    b. At the end of **3'**, the program will do part (a) automatically, measuring the net extension required to achieve preload and adding it to the initial Grips Gage Length. Extension will then reset to zero.

36. Calculate the **2% strain** displacement (extension) value from the Adjusted Gage Length and write it down on the test sheet.

37. MTS will calculate **2% strain** extension magnitude as the target strain and run the stress relaxation program, holding the strain for a total of **25'**.

a. When the tendon reaches **2% strain**, start a stopwatch and take a B-mode and SWE image (images at peak stress) on the US machine.

b. After **20'**, take another B-mode and SWE image (images at relaxed/equilibrium stress) on the US machine and note the load measurement at this point on the test sheet.

c. After successive **2'** cycles, take another B-mode and SWE image on the US machine and note the load measurement at this point on the test sheet.

d. The crosshead will return to the Gage Length so that there is no load for **20'**, allowing the tendon to recover.

e. Save the raw data.

38. Input the **4% strain** value as the target strain and run the stress relaxation program, repeating steps 34-37

39. Input the **6% strain** value as the target strain and run the stress relaxation program, repeating steps 34-37

40. Input the **8% strain** value as the target strain and run the stress relaxation program, repeating steps 34-37

41. Save the test file.

42. On TWE select the stress relaxation template labeled SLH_PTF.

a. Start the program. Input measured Width, Thickness, and Grips Gage Length.

b. During preloading, take a BMode and SWE image on the US machine.

c. The load will increase to **2 N** and hold the resulting extension for **3'** to overshoot the desired preload value of **1 N**. Write down this extension as displayed as Preload Additional Length. Add Grips Gage Length to Preload Additional Length to get Adjusted Gage Length.

d. At the end of **3'**, the program will do part (a) automatically, measuring the net extension required to achieve preload and adding it to the initial Gage Length. Extension will then reset to zero.

e. After preloading, MTS will raise the crosshead at 0.5 mm/s until failure is achieved. Capture a 60s prospective B-mode video on the US machine while this is happening by pressing the "Save Clip" button when the crosshead begins to rise.

43. Proceed to Phase 4.

Phase 3c – Damage Pull

44. On TWE select the stress relaxation template labeled SLH_SR.

45. Start the program. Input measured Width, Thickness, and Grips Gage Length. During preloading, take a BMode and SWE image on the US machine.

a. The load will increase to **2 N** and hold the resulting extension for **3'** to overshoot the desired preload value of **1 N**. Write down this extension as displayed as Preload Additional Length. Add Grips Gage Length to Preload Additional Length to get Adjusted Gage Length.

      b. At the end of **3'**, the program will do part (a) automatically, measuring the net extension required to achieve preload and adding it to the initial Grips Gage Length. Extension will then reset to zero.

46. Calculate the **2% strain** displacement (extension) value from the Adjusted Gage Length and write it down on the test sheet.

47. MTS will calculate **2% strain** extension magnitude as the target strain and run the stress relaxation program, holding the strain for a total of **20'**.
    a. When the tendon reaches **2% strain**, start a stopwatch and take a B-mode and SWE image (images at peak stress) on the US machine.
    b. After **19.5'**, take another B-mode and SWE image (images at relaxed/equilibrium stress) on the US machine and note the load measurement at this point on the test sheet.
    c. The crosshead will return to the Gage Length so that there is no load for **20'**, allowing the tendon to recover.
    d. Save the raw data and test file.

48. Locate and start the TWE program labeled SLH_Damage_Pull.

49. Repeat steps 45-46 for **10% strain**.

50. After preloading, the program will execute one cycle of **10% strain** at **1/3 Hz**. With the tendon returned to slack (crosshead = 0), allow the tendon to recover for **20'**

51. After the **20'** rest period, repeat steps 44-47. At this point the tendon has experienced two stress relaxations at **2% strain** with a damage pull at **10% strain** in between.

52. On the hand controller, increase the crosshead to preload (**2 N**) *OR* select any of the above programs to run just the preload protocol (step 45). Take a BMode and SWE image on the US machine.

53. Proceed to Phase 4

Phase 4 – Clean-up

54. Move the crosshead down so that the sample is in slack.

55. Using the tube attached to the tank, drain the saline from the tank into a waste bucket.

56. Use a large sponge to drain any remaining saline from the bottom of the tank into the waste bucket

57. Dispose of the waste saline in the sink.

58. Remove the 8-32 kep nuts to disengage the grips from the grip-mounts.

59. Move the tendon and grips back to the absorbent pad/cutting board and remove the 8-32 socket head screws to release the tendon-dacron complex from the grips. Dispose of the specimen in a biohazard waste bag.

60. Unscrew and remove the bottom grip-mount.

61. Unscrew and remove the plastic nut and o-ring in the compression seal.

62. Using a wrench, loosen the jam nut on the insert. Turn the top grip-mount CW to release the insert pin. Remove the insert from the load cell.

63. Unscrew the insert from the threaded rod.

64. Loosen the jam nut on the grip-mount. Unscrew the M6 threaded rod from the grip-mount. At this point the pin, insert, threaded rod, and grip-mount should all be separated.
65. Wipe down the tank with paper towels so that it is dry and remove the tank extender.
66. Spray the inside of the tank with ethanol and wipe down.
67. Wash grip-mounts and grips.

Appendix C – Mechanical Analysis Code

StressRelaxationAnalysis.mlx

This program reads an excel sheet for MTS data and for each stress relaxation outputs the %relaxation and Equilibrium Modulus

```
clear
clc


% Read the Excel data
filename = 'SDFT.15.3-13-25.xlsx';
data = readmatrix(filename);


testtype = input('SR or DP? ','s');


if testtype == "SR"
    stresslevel2 = data(:, 13); % 2 SR
    strainlevel2 = data(:, 12); % 2 SR
    stresslevel4 = data(:, 19); % 4 SR
    strainlevel4 = data(:, 18); % 4 SR
    stresslevel6 = data(:, 25); % 6 SR
    strainlevel6 = data(:, 24); % 6 SR
    stresslevel8 = data(:, 31); % 8 SR
    strainlevel8 = data(:, 30); % 8 SR
end


if testtype == "DP"
    stresslevel2init = data(:, 13);
    strainlevel2init = data(:, 12);
    stresslevel2final = data(:, 25);
    strainlevel2final = data(:, 24);
end


% default color preferences
maroon = "#861F41";
orange = "#E5751F";


if testtype == "SR"
    j = 1;
    for i = 1:length(strainlevel2)
        if strainlevel2(i) >= 0.0199
```

```matlab
            relaxation2(j) = stresslevel2(i);
            j = j + 1;
        end
        if i > 12000
            if strainlevel2(i) >= 0.0199
                stress2(j) = stresslevel2(i);
                strain2(j) = strainlevel2(j);
            end
        end
end
M2 = movmean(relaxation2, 500);
figure(1);
plot(relaxation2);
title('2% Strain - SR');
ylabel('Stress [MPa]');
hold on
plot(M2);
percent_relax_2 = 100*(min(M2) - max(M2))/max(M2);
Eeq_2 = min(M2)/0.02; % Equilibrium Modulus


j = 1;
for i = 1:length(strainlevel4)
    if strainlevel4(i) >= 0.0399
        relaxation4(j) = stresslevel4(i);
        j = j + 1;
    end
end
M4 = movmean(relaxation4, 500);
figure(2);
plot(relaxation4);
title('4% Strain - SR');
ylabel('Stress [MPa]');
hold on
plot(M4);
percent_relax_4 = 100*(min(M4) - max(M4))/max(M4);
Eeq_4 = min(M4)/0.02; % Equilibrium Modulus


j = 1;
for i = 1:length(strainlevel6)
    if strainlevel6(i) >= 0.0599
        relaxation6(j) = stresslevel6(i);
        j = j + 1;
    end
end
M6 = movmean(relaxation6, 500);
```

```matlab
    figure(3);
    plot(relaxation6);
    title('6% Strain - SR');
    ylabel('Stress [MPa]');
    hold on
    plot(M6);
    percent_relax_6 = 100*(min(M6) - max(M6))/max(M6);
    Eeq_6 = min(M6)/0.02; % Equilibrium Modulus


    j = 1;
    for i = 1:length(strainlevel8)
        if strainlevel8(i) >= 0.0799 % only keep stress values for strains above
8%
            relaxation8(j) = stresslevel8(i);
            j = j + 1;
        end
    end
    M8 = movmean(relaxation8, 500);
    figure(4);
    plot(relaxation8);
    title('8% Strain - SR');
    ylabel('Stress [MPa]');
    hold on
    plot(M8, 'color', );
    percent_relax_8 = 100*(min(M8) - max(M8))/max(M8);
    Eeq_8 = min(M8)/0.02; % Equilibrium Modulus


    figure(5);
    combinedData = [M2,M4,M6,M8];
    plot(combinedData,'Color',maroon,'LineWidth',3);
    title('Concatenated SRs');
    ylabel('Stress [MPa]');


    figure(6);
    combinedStress = [stresslevel2;stresslevel4;stresslevel6;stresslevel8];
    Mcombined = movmean(combinedStress, 10);
    combinedStrain = [strainlevel2;strainlevel4;strainlevel6;strainlevel8];
    for i=1:length(combinedStrain)
        if combinedStrain(i) > 0
            cleanedStress(j) = Mcombined(i);
            cleanedStrain(j) = combinedStrain(i);
```

```matlab
                j = j + 1;
        end
    end
    p1 = plot(cleanedStrain,cleanedStress, 'Color', "#861F41", 'LineWidth', 3);
    hold on
    p2 = plot([0, 0.02], [0, min(M2)],':','Color',"#E5751F", 'LineWidth',3);
    plot([0.02, 0.04], [min(M2), min(M4)],':','Color',"#E5751F", 'LineWidth',3);
    plot([0.04, 0.06], [min(M4), min(M6)],':','Color',"#E5751F", 'LineWidth',3);
    plot([0.06, 0.08], [min(M6), min(M8)],':','Color',"#E5751F", 'LineWidth',3);
    title('SDFT #15 Stress-Strain Curve - Stress Relaxation');
    ylabel('Stress [MPa]');
    xlabel('Strain [mm/mm]');
    legend([p1, p2], {'Data','Eq Stress vs. Eq Strain'},'Location','northwest');

    % Distance Formula on stress-strain plot
    M2_modulus = (min(M2) - 0)/(0.02 - 0);
    M4_modulus = (min(M4) - min(M2))/(0.04 - 0.02);
    M6_modulus = (min(M6) - min(M4))/(0.06 - 0.04);
    M8_modulus = (min(M8) - min(M6))/(0.08 - 0.06);
end


if testtype == "DP"
    j = 1;
    for i = 1:length(strainlevel2init)
        if strainlevel2init(i) >= 0.0199 % only keep stress values for strains
above 2%
            relaxation2init(j) = stresslevel2init(i);
            j = j + 1;
        end
    end
    Minit = movmean(relaxation2init, 500);
    figure(1);
    plot(relaxation2init);
    hold on
    plot(Minit);
    title('Initial Stress Relaxation');
    ylabel('Stress [MPa]');
    percent_relax_2init = 100*(min(Minit) - max(Minit))/max(Minit); % Percent
Relaxation
    Eeq_2init = min(Minit)/0.02; % Equilibrium Modulus


    j = 1;
    for i = 1:length(strainlevel2final)
        if strainlevel2final(i) >= 0.0199 % only keep stress values for strains
above 2%
```

```matlab
            relaxation2final(j) = stresslevel2final(i);
            j = j + 1;
        end
    end
    Mfinal = movmean(relaxation2final, 500);
    figure(2);
    plot(relaxation2final);
    hold on
    plot(Mfinal);
    title('Final Stress Relaxation');
    ylabel('Stress [MPa]');
    percent_relax_2final = 100*(min(Mfinal) - max(Mfinal))/max(Mfinal); % Percent
Relaxation
    Eeq_2final = min(Mfinal)/0.02; % Equilibrium Modulus
end
```

YieldAnalysis_SlopeMethod.mlx

```matlab
% Import Data
% Import CSV or Excel file
clc; clearvars; close all;
[mtsfile, mtspath] = uigetfile({
    '*.csv;*.CSV', 'CSV tables (*.csv)';
    '*.xls;*.xlsx', 'Excel workbooks (*.xls, *.xlsx)';
}, "Select MTS failure data");
data = readmatrix(strcat(mtspath, mtsfile));


% Generate folder for output plots
outputFolder = 'Output Plots/';
if isfolder(outputFolder)
    disp('Output folder exists'); % this doesn't go to cmd window in mlx for some
reason
else
    mkdir(outputFolder);
    disp('Output folder was not found, generated new one in current MATLAB
folder');
end


% Prompt for and save sample index
promptmnumber = "What sample number? ";
samplenumber = input(promptmnumber);
sample = ['SDFT.', num2str(samplenumber)];
sample = string(sample);


startIndex = 1; % where the data starts in the mts export file
```

```
% Assign variables from CSV import, check on each new MTS session that this
% is the correct column assignment
mtsdata.time =              data(startIndex:end, 1);
mtsdata.crosshead =         data(startIndex:end, 2);
mtsdata.ext =               data(startIndex:end, 3);
mtsdata.load =              data(startIndex:end, 4); % replaced in Strain
Correction step
mtsdata.strain =            data(startIndex:end, 5); % replaced in Stress
Correction step
mtsdata.stress =            data(startIndex:end, 6); % replaced in Stress
Correction step
```

CSA Calculation

Prompts to manually input physical sample measurements made before PTF Test

```
% promptw = "Width? ";
% width = input(promptw);
% promptt = "Thickness? ";
% thickness = input(promptt);
% promptGL = "PTF Gage Length? ";
% initial_GL = input(promptGL);


% csa = (pi*thickness*width)/4; % [mm^2], elliptical cross sectional area
approximation
```

Populate MTS data and required parameters

Automatic version for data that doesn't need to recalculate csa

```
% convert mts structure to arrays
stress = mtsdata.stress; % [MPa]
strain = mtsdata.strain;
csa = stress(1)/mtsdata.load(1); % [mm^2], cross-sectional area backed out from
stress and load


% Stretch Ratio Calculation
initial_GL = mtsdata.ext(1)/strain(1); % [mm], gage length backed out from
extension and strain
stretch_ratio = (initial_GL+mtsdata.crosshead)/initial_GL;
```

Differentiating Smooth Stress v. Strain Curve

The main objective of this section is to identify the yield point, which is the maximum slope of the stress v. strain plot

```
maxStress = max(stress);
maxStressIndex = find(stress == maxStress);
```

```matlab
strainAtMaxStress = strain(maxStressIndex); % {SLH - changed "MaxStrain" to
"strainAtMaxStress"}


% generate region for yield point search
toeregion = find(stress > 0.35*maxStress); % Yield point must be greater than 30%
of max load to put us out of toe region
toeregionInd = toeregion(1,1); % Mark the end of the toe region
stretch2peak = stretch_ratio(toeregionInd:maxStressIndex,1); % subset of stretch
ratio between the end of the toe region and max load
stress2peak = stress(toeregionInd:maxStressIndex,1); % subset of stress between
the end of the toe region and max stress


% fit a smooth spline to data between the toe region and max stress
spline1= fit(stretch2peak, stress2peak, 'smoothingspline', 'SmoothingParam',
0.9999); % can change final value to make the curve smoother/rougher


% find first derivative of smooth spline
[r1,r2] = differentiate(spline1, stretch2peak); % dload/dstretch
[yieldy, yieldindex] = max(r1); % yield occurs at the maximum stiffness in the
linear region
yieldx= stretch2peak(yieldindex); % yield stretch ratio
yieldy_stress= stress2peak(yieldindex); % yield stress [MPa]
```

Elastic Modulus based on MAX load

```matlab
p = .3; % linear regression must include > 30% of data
[maxLoad, maxLoadIndex] = max(mtsdata.load);
ExtAtMaxLoad = mtsdata.crosshead(maxLoadIndex);
index = maxLoadIndex; % index to stop at (usually max load or yield load)
start = max(round(0*index), 1); % ignore first x% (pre-processing)
load = mtsdata.load(start:index); % load from start to max load
ext = mtsdata.crosshead(start:index); % crosshead from start to max load
l = length(ext); % # of timesteps to maximum
w = round(p*l); % 30% of l, give or take


% Stiffness from Load vs. Extension (crosshead)
s_guess = (load(w+1:end) - load(1:l-w))./(ext(w+1:end) - ext(1:l-w)); % the slope
of all possible lines w wide from start to max load
[s, t] = max(s_guess); % max slope region, w wide, may not include max load since
LvE graph begins to flatten near maximum load
b_s = load(t) - s*ext(t); % y-intercept of selected maximum slope line
Stiffness = s; % interpretation, [N/mm]


% Modulus from Stress vs. Strain
```

```matlab
m_guess = (stress(w+1:l) - stress(1:l-w))./(strain(w+1:l) - strain(1:l-w)); % the
slope of all possible lines w wide from start to max stress
[m, n] = max(m_guess);
b_m = stress(n) - m*strain(n);
Modulus = m; % interpretation, [MPa]


% create regression lines
regy_s = s.*ext + b_s;
regy_m = m.*strain + b_m;


% determine stiffness R^2
resid = load(t:t+w) - regy_s(t:t+w);
SSresid = sum(resid.^2);
SStotal = (l - 1)*var(load);
rsq = 1 - SSresid/SStotal;
StiffnessRSQ = rsq;


% determine modulus R^2
yresid_m = stress(t:t+w) - regy_m(t:t+w);
SSresid_m = sum(yresid_m.^2);
SStotal_m = (l - 1)*var(stress(start:index));
rsq_m = 1 - SSresid_m/SStotal_m;
ModulusRSQ = rsq_m;
```

Elastic Modulus based on YIELD load

```matlab
yieldInd= yieldindex+toeregionInd; % add toe region indexes back to total yield
index
yindex = yieldInd; % index to stop at (usually max load or yield load)
ystart = max(round(0*yindex), 1); % ignore first x% (pre-processing)
yload = mtsdata.load(ystart:yindex); % load from start to yield load
yext = mtsdata.crosshead(ystart:yindex); % crosshead from start to yield load
l_y = length(yext); % # of timesteps to maximum
w_y = round(p*l_y); % 30% of l, give or take


% Stiffness from Load vs. Extension (crosshead)
s_guess_y = (yload(w_y+1:end) - yload(1:l_y-w_y))./(yext(w_y+1:end) - yext(1:l_y-
w_y)); % the slope of all possible lines w wide from start to yield load
[s_y, t_y] = max(s_guess_y); % max slope region, w wide
b_s_y = yload(t_y) - s_y*yext(t_y); % y-intercept of selected maximum slope line
TruncatedStiffness = s_y; % interpretation, [N/mm]


% Modulus from Stress vs. Strain
```

```matlab
m_guess_y = (stress(w_y+1:l_y) - stress(1:l_y-w_y))./(strain(w_y+1:l_y) -
strain(1:l_y-w_y)); % the slope of all possible lines w wide from start to yield
stress
[m_y, n_y] = max(m_guess_y);
b_m_y = stress(n_y) - m_y*strain(n_y);
TruncatedModulus = m_y; % interpretation, [MPa]


% create regression lines
regy_s_y = s_y.*yext + b_s_y;
regy_m_y = m_y.*strain + b_m_y;


% determine stiffness R^2
yresid = yload(t_y:t_y+w_y) - regy_s_y(t_y:t_y+w_y);
SSresid_y = sum(yresid.^2);
SStotal_y = (l_y - 1)*var(yload);
rsq_y = 1 - SSresid_y/SStotal_y;
TruncatedStiffnessRSQ = rsq_y;


% determine modulus R^2
yresid_m = stress(t_y:t_y+w_y) - regy_m_y(t_y:t_y+w_y);
SSresid_m_y = sum(yresid_m.^2);
SStotal_m_y = (l_y - 1)*var(stress(ystart:yindex));
rsq_m_y = 1 - SSresid_m_y/SStotal_m_y;
TruncatedModulusRSQ = rsq_m_y;
```

Graphs

```matlab
% Load vs. Extension with max point and modulus sample based on max
figure(1)
plot(mtsdata.crosshead, mtsdata.load)
hold on
plot(ext(t:t+w), regy_s(t:t+w)) % {SLH - changed "index" to "n+w"}
plot(mtsdata.crosshead(index), mtsdata.load(index), "xr") % plot max load point
hold off
title("Load vs Extension");
xlabel("Extension (mm)"); ylabel("Load (N)");
filename = append(sample, '_LvE_regline_maxpoint.png');
path = append('Output Plots/',filename);
exportgraphics(figure(1),path);


% Load vs. Extension with yield point and modulus sample based on yield
figure(2)
plot(mtsdata.crosshead, mtsdata.load)
hold on
plot(yext(t_y:t_y+w_y), regy_s_y(t_y:t_y+w_y))
```

```matlab
plot(mtsdata.crosshead(yindex), mtsdata.load(yindex), "*g") % plot yield load
point
hold off
title("Load vs Extension");
xlabel("Extension (mm)"); ylabel("Load (N)");
filename = append(sample, '_LvE_regline_yieldpoint.png');
path = append('Output Plots/',filename);
fig = gcf;
exportgraphics(fig,path);


% Stretch Ratio vs. Stress with yield point
figure(3)
plot(stretch_ratio, stress)
hold on
plot(yieldx, yieldy_stress, '*g')
hold off
xlabel("Stretch Ratio (\lambda)")
ylabel("Stress (\sigma, kPa)")
filename = append(sample, '_StressvStretchRatio_yieldpoint.png');
path = append('Output Plots/',filename);
fig = gcf;
exportgraphics(fig,path);


% Smoothed spline on data with yield point
% Overlaid on Stretch Ratio vs. Stress
figure(4)
plot(stretch2peak, stress2peak, 'k')
hold on
plot(spline1, stretch2peak, stress2peak, 'b')
plot(yieldx, yieldy_stress, '*g')
hold off
xlabel("Stretch Ratio")
ylabel("Stress (MPa)")
legend('data','data points','spline','yield point','Location','southeast')
filename = append(sample, '_StressvStretchRatio_spline.png');
path = append('Output Plots/',filename);
fig = gcf;
exportgraphics(fig,path);


% Derivative of spline vs. Stretch Ratio, largest value is yield point
figure(5)
plot(stretch2peak, r1)
hold on
plot(yieldx, yieldy, '*g')
hold off
```

```matlab
xlabel("Stretch Ratio (\lambda)")
ylabel("d\sigma/d\lambda")
filename = append(sample, '_DStressDStretchRatio.png');
path = append('Output Plots/',filename);
fig = gcf;
exportgraphics(fig,path);


% Stress vs. Strain with max point and modulus sample based on max
figure(6)
plot(strain,stress)
hold on
plot(strain(n:n+w), regy_m(n:n+w))
plot(strain(index), stress(index), "xr") % plot max load point
hold off


title("Stress vs. Strain", sample);
xlabel("Strain [mm/mm]"); ylabel("Stress [MPa]");
xlim([0 0.11]);
filename = append(sample, '_StressvStrain_regline_maxpoint.png');
path = append('Output Plots/',filename);
fig = gcf;
exportgraphics(fig,path);


% Stress vs. Strain with yield point and modulus sample based on yield
figure(7)
plot(strain,stress)
hold on
plot(strain(n_y:n_y+w_y), regy_m_y(n_y:n_y+w_y))
plot(strain(yindex), stress(yindex), "*g") % plot yield load point
hold off
title("Stress vs. Strain", sample);
xlabel("Strain [mm/mm]"); ylabel("Stress [MPa]");
xlim([0 0.11]);
filename = append(sample, '_StressvStrain_regline_yieldpoint.png');
path = append('Output Plots/',filename);
fig = gcf;
exportgraphics(fig,path);
```

Output Table

Gather Outputs

```matlab
yieldStress = yieldy_stress;
yieldLoad= mtsdata.load(yieldInd);
strainAtYield = strain(yieldInd);
ExtAtYield = mtsdata.crosshead(yieldInd);
```
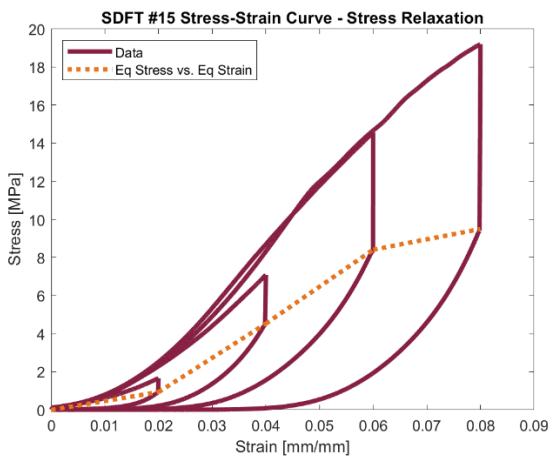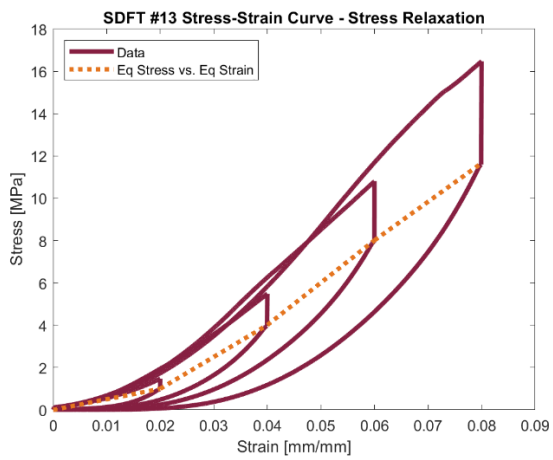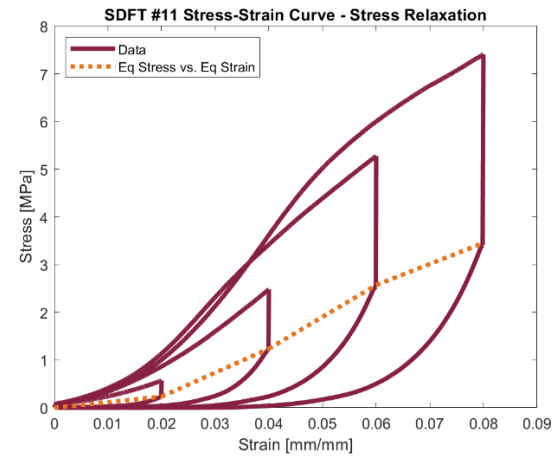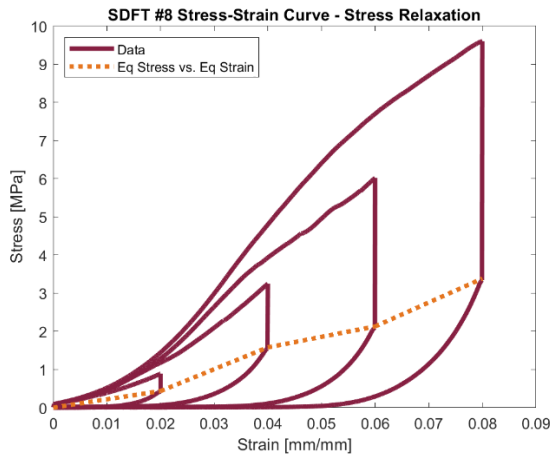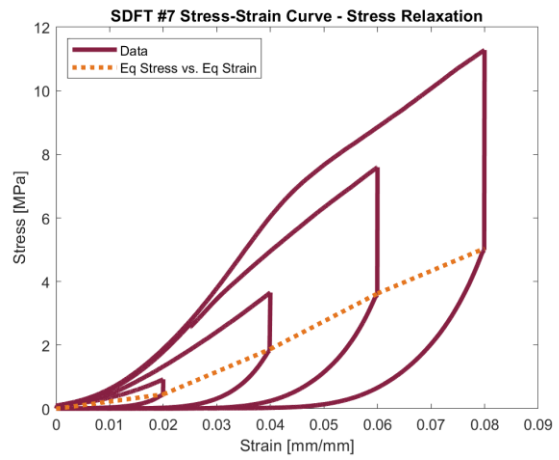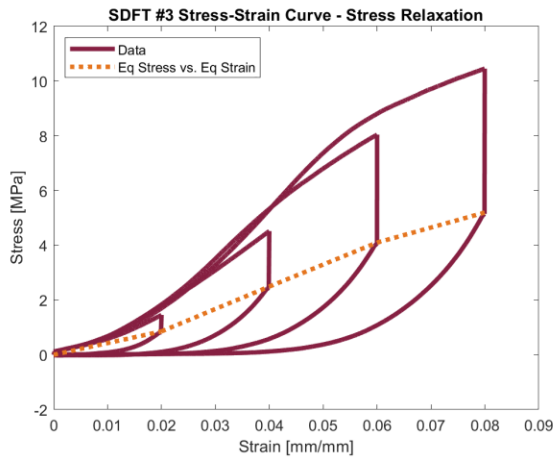
```matlab
PostYieldExt = mtsdata.crosshead(maxLoadIndex) - mtsdata.crosshead(yieldInd);
PostYieldStrain = strain(maxLoadIndex) - strain(yieldInd);
NormalizedYieldLoad = yieldLoad/maxLoad;
ExtAtMax = mtsdata.crosshead(maxLoadIndex);
NormExtAtYield = ExtAtYield/ExtAtMax;
NormPYE = PostYieldExt/ExtAtMax;


% Trapezoidal integration for work and energy
WorkToYield = trapz(mtsdata.crosshead(1:yieldInd), mtsdata.load(1:yieldInd));
WorkToMax = trapz(mtsdata.crosshead(1:maxLoadIndex),
mtsdata.load(1:maxLoadIndex));
EnergytoYield = trapz(strain(1:yieldInd), stress(1:yieldInd));
EnergytoMax = trapz(strain(1:maxLoadIndex), stress(1:maxLoadIndex));
WorkRatio = WorkToYield/WorkToMax;
EnergyRatio = EnergytoYield/EnergytoMax;


% Output to Excel table
output= table(sample, csa, initial_GL, maxLoad, yieldLoad, maxStress,
yieldStress, strainAtMaxStress, strainAtYield, PostYieldStrain, ExtAtYield,
PostYieldExt, Stiffness, StiffnessRSQ, Modulus, ModulusRSQ, TruncatedStiffness,
TruncatedStiffnessRSQ, TruncatedModulus, TruncatedModulusRSQ, WorkToYield,
WorkToMax, EnergytoYield, EnergytoMax);
filenameexp = 'MechDataforSDFTPTF.xlsx';
writetable(output,filenameexp,'Sheet',1,'WriteVariableNames',true,'WriteMode','ap
pend'); % WriteVariableNames should only be "true" the first run
```

Appendix D – Additional Figures

SDFT #1

SDFT #2

SDFT #4

SDFT #9

SDFT #14

SDFT #16

SDFT #17

Stress vs. Strain

SDFT #18

Stress vs. Strain
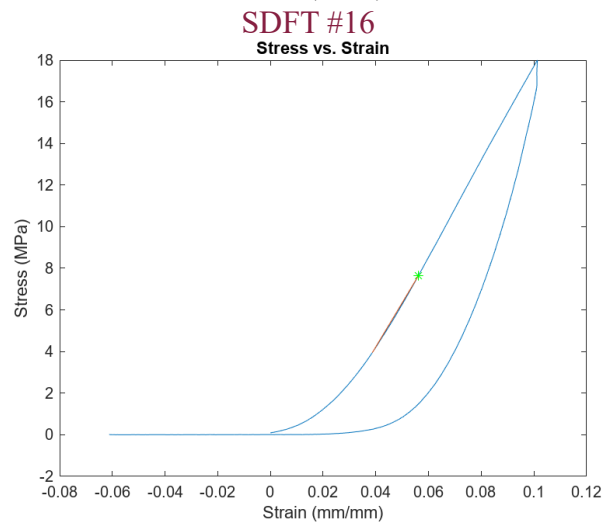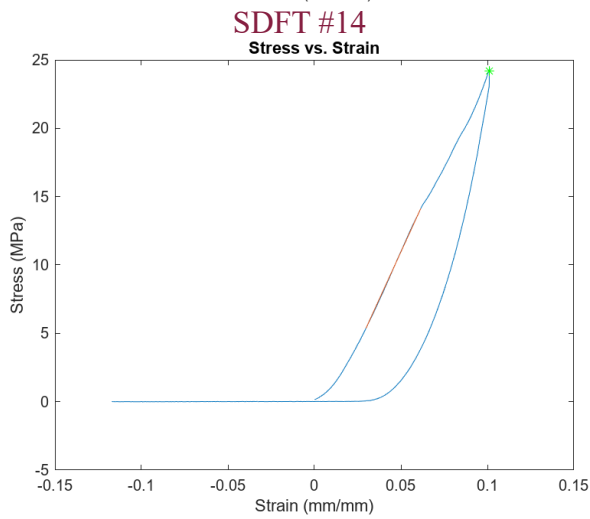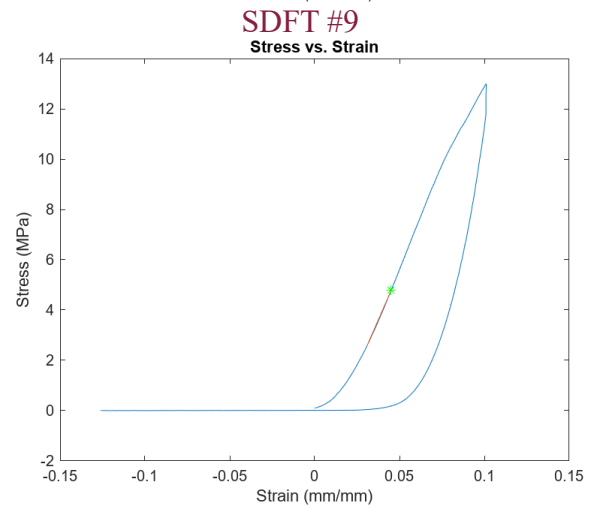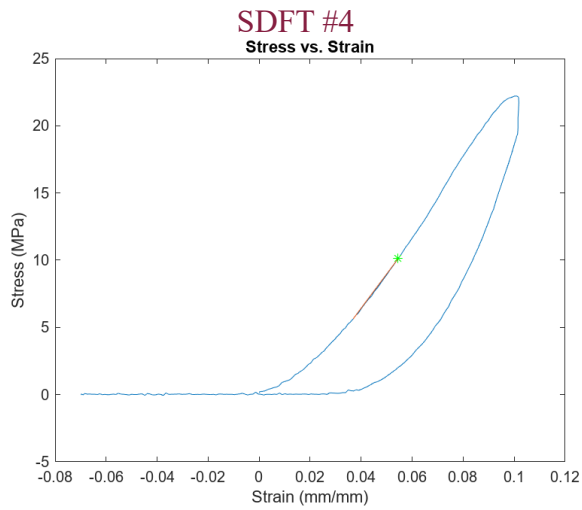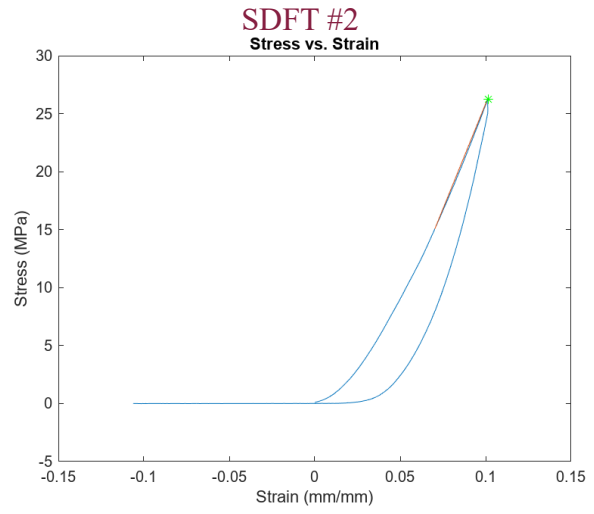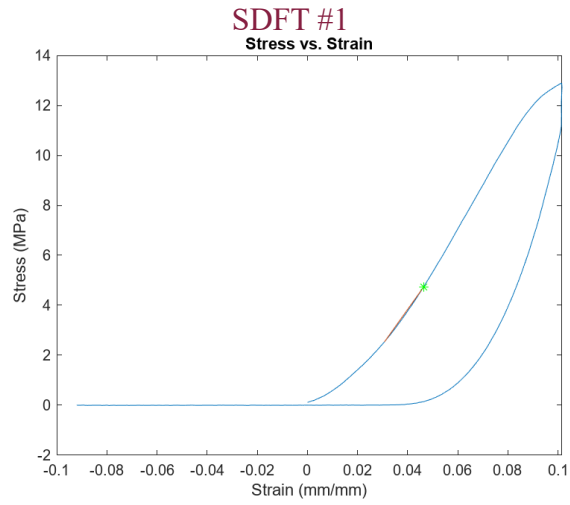
Appendix E – Radiomic Analysis Code

AllRadiomics.py

```python
1    import SimpleITK as sitk
2    import numpy as np
3    import pandas as pd
4    import matplotlib.pyplot as plt
5    from radiomics import featureextractor
6    import warnings
7    from PIL import Image
8
9
10   def textureAnalysisDICOM(imgFile, imgFileString, segmentationPath,
printOutput=False, saveOutput=False, outputFilename=None):
11       try:
12           # Convert three channel RGB to single channel grayscale to match
the image mask
13           grayscale_array = imgFile.dot([0.07, 0.72, 0.21])  # convert RGB
image to grayscale
14           cropped_array = grayscale_array[218:894, 249:1153]  # crop the
UI
15           img = sitk.GetImageFromArray(cropped_array)
16           segmentationImg = sitk.ReadImage(segmentationPath)
17
18           # When experimenting with the .nrrd, .jpeg, and .png conversions
I occasionally ran
19           # into a dimension related error, but in the final build I
wasn't so I put this in as a safeguard.
20           if img.GetDimension() != segmentationImg.GetDimension():
21               print("\033[91m" + "\nIf you are seeing this message then
there is a dimension related problem. If you"
22                                   "reach out to Gabe I have a solution for
this, but I didn't think it was "
23                                   "needed at the time." + "\033[0m")
24           print("Segmentation dimensions:",
segmentationImg.GetDimension())
25           print("Image dimensions:", img.GetDimension())
26
27           # Here is where you will customize how you want to perform the
TA. If you want to make any changes to
28           # this I recommend reading the PyRadiomics documentation.
29           extractor = featureextractor.RadiomicsFeatureExtractor()
30           extractor.enableFeatureClassByName('firstorder')
31           extractor.enableFeatureClassByName('shape2D')
32           extractor.enableFeatureClassByName('glcm')
33           extractor.enableFeatureClassByName('gldm')
34           extractor.enableFeatureClassByName('glrlm')
35           extractor.enableFeatureClassByName('glszm')
36           extractor.enableFeatureClassByName('ngtdm')
37           extractor.settings['geometryTolerance'] = 1
38           extractor.settings['force2D'] = True
39
```
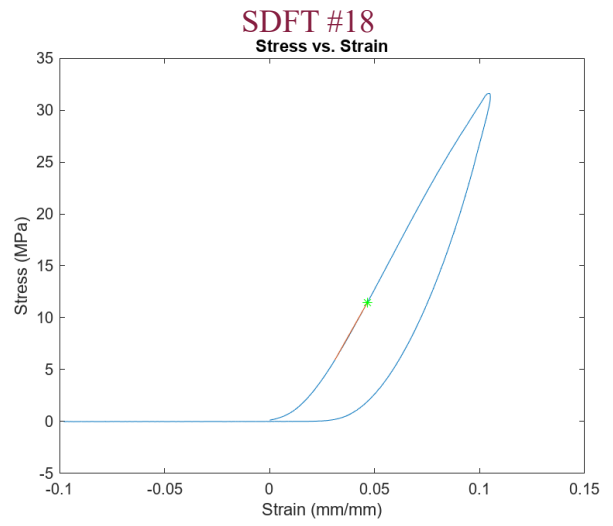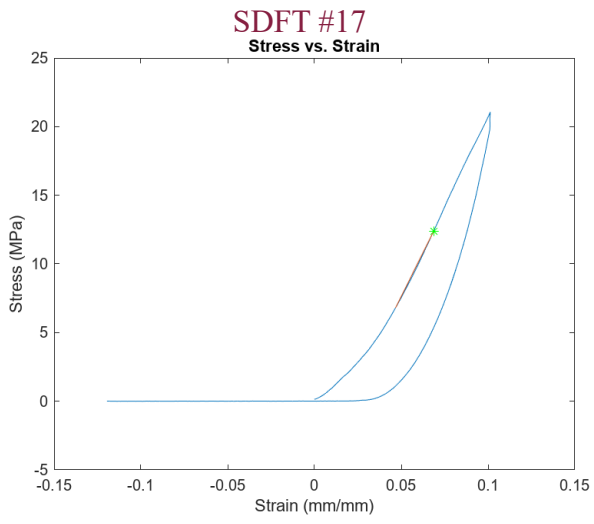
```
40          # I tossed in this warnings ignorer since PyRadiomics likes to
print a lot of information that clogs up
41          # the terminal. If you want, feel free to comment it out.
42          with warnings.catch_warnings():
43              warnings.simplefilter("ignore")
44              # Label map error can be fixed here (changing the value for
label=____)
45              parameters = extractor.execute(img, segmentationPath,
label=255)
46
47          # Saves all the parameters to a pandas dataframe
48          parametersDF = pd.DataFrame(parameters.items())
49          parametersDF = parametersDF.T
50
51          header_row = 0
52          parametersDF.columns = parametersDF.iloc[header_row]
53          parametersDF = parametersDF.drop(range(1))
54
55          # adding a column for the filename and moving it to the front
56          parametersDF['Filename'] = imgFileString
57          columns = ['Filename'] + [col for col in parametersDF.columns if
col != 'Filename']
58          parametersDF = parametersDF[columns]
59
60          if printOutput:
61              print(parametersDF)
62
63          if saveOutput:
64              if outputFilename is not None:
65                  parametersDF.to_csv(outputFilename, mode='a',
index=True, header=True)
66
67          print("\033[92m" + "Successfully calculated texture analysis
features (JPEG/PNG approach)" + "\033[0m")
68          return parametersDF
69
70      except Exception as e:
71          # This will print the specific error message if anything does go
wrong with the TA
72          print("\033[91m" + "\nFailed to extract texture analysis
features" + "\033[0m")
73          print("\033[91m" + f"Error Message:{e}" + "\033[0m")
74
75
76  def getSWEStats(SWECompositeMap, maxshearwavespeed):
77      img = Image.open(SWECompositeMap)
78      rgb_img = np.array(img)
79
80      # Step 1: Create colormap with 900 entries
81      jet_colormap = plt.cm.get_cmap('jet', 900)
82      cmap = jet_colormap(np.arange(900))[:, :3]  # Remove alpha channel
83
84      # Step 2: Map colormap indices to intensity values (0-255)
85      intensity_scale = np.linspace(0, 255, 900).astype(np.uint8)
86
87      # Step 3: Flatten the RGB image for efficient processing
88      rgb_img_flattened = rgb_img.reshape(-1, 3)  # Shape: (num_pixels, 3)
```

```
89
90       # Step 4: Find the closest matching colormap index for each pixel
91       indices = np.argmin(np.linalg.norm(rgb_img_flattened[:, None, :] -
cmap[None, :, :], axis=2), axis=1)
92
93       # Step 5: Map the indices to grayscale intensities
94       grayscale_img = intensity_scale[indices].reshape(rgb_img.shape[:2])
# Reshape back to (height, width)
95
96       # Result: Grayscale image with values between 0-255
97       print(grayscale_img.shape)  # (height, width)
98
99       plt.figure(figsize=(10, 5))
100      plt.subplot(1, 2, 1)
101      plt.imshow(rgb_img)
102      plt.title("Original RGB Image")
103      plt.axis('off')
104
105      plt.subplot(1, 2, 2)
106      plt.imshow(grayscale_img, cmap='gray')
107      plt.title("Grayscale from Jet Colormap")
108      plt.axis('off')
109
110      plt.show()
111
112      # Filter out zero values
113      non_zero_values = grayscale_img[grayscale_img > 0]
114
115      sws = non_zero_values * maxshearwavespeed / 255
116      avg_sws = np.mean(sws, axis=0)
117      max_sws = np.max(sws, axis=0)
118      tissuedensity = 1120  # kg/m3, Ker (1981)
119
120      modulus = 3 * tissuedensity * (sws**2)
121      avg_modulus = np.mean(modulus, axis=0)
122
123      print(avg_sws, max_sws, avg_modulus)
```

<div align="center">imageAnalysis.py</div>

```
1    import matplotlib.pyplot as plt
2    import pydicom as dicom
3    import os
4    from PIL import Image
5
6    from segmentFunctions import autosegment
7    from allRadiomics import textureAnalysisDICOM, getSWEStats
8
9    plt.close('all')
10
11   images = {}  # preload a dictionary for the raw image and its altered
forms
12   imageFolder = r'E:\US Images\SDFT.17.3-23-25'  # modify this to switch
set that is analyzed
13   segmentFolder = r'E:\US Images\Segments'
14   outputFolder = r'E:\US Images\Output'
```

```
15    files = os.listdir(imageFolder)
16    maxshearwavespeed = 16.3  # m/s, check images each iteration
17
18    for imageFile in files:
19        inputImagePath = os.path.join(imageFolder, imageFile)
20
21        imageFileString = str(imageFile)
22        print(imageFile)
23        ds = dicom.dcmread(inputImagePath)
24        images[imageFile] = ds.pixel_array
25
26        pixels = autosegment(images[imageFile], imageFile)
27        segment = Image.fromarray(pixels)
28        segmentPath = os.path.join(segmentFolder,
os.path.splitext(imageFile)[0] + '.png')
29        segment.save(segmentPath)
30        print(imageFile, ' segment saved')
31
32        outputFile = os.path.basename(imageFolder)
33        outputFilePath = os.path.join(outputFolder, outputFile + ' Radiomics
Analysis.csv')
34        if "SWE" in imageFile:
35            # This part is extremely computationally expensive, consider
running B images in a separate analysis for speed
36            print("Shear Wave not analyzed")
37            #getSWEStats(segmentPath, maxshearwavespeed)
38        if "SWE" not in imageFile:
39            textureAnalysisDICOM(images[imageFile], imageFileString,
segmentPath, printOutput=True, saveOutput=True,
40                                 outputFilename=outputFilePath)
```

segmentFunctions.py

```
1    import numpy as np
2    from skimage import measure, morphology
3    from scipy import ndimage
4
5
6    def threshold_py(image, threshold):
7        return image > threshold
8
9
10   def autosegment(rawInput, filename):
11       pixels = {}
12
13       if "SWE" not in filename:
14           pixels['grayscale'] = rawInput.dot([0.07, 0.72, 0.21])  #
convert RGB image to grayscale
15           pixels['cropped'] = pixels['grayscale'][218:894, 249:1153]  #
crop the UI
16
17           threshold = 100  # pixels with lower intensity than this value
are removed
18           pixels['thresholded'] = threshold_py(pixels['cropped'],
threshold)
19
```

```
20              # separate main tendon from other structures
21              sq = morphology.square(width=3)
22              dia = morphology.diamond(radius=1)
23
24              pixels['opened1'] =
morphology.binary_erosion(pixels['thresholded'], dia)
25              pixels['opened2'] = morphology.binary_erosion(pixels['opened1'],
dia)
26              pixels['opened3'] = morphology.binary_erosion(pixels['opened2'],
dia)
27
28              pixels['closed1'] =
morphology.binary_dilation(pixels['opened3'], sq)
29              pixels['closed2'] =
morphology.binary_dilation(pixels['closed1'], sq)
30
31              # label and calculate properties for every cluster in mask
32              pixels['labeled'] = measure.label(pixels['closed2'])
33              rp = measure.regionprops(pixels['labeled'])
34
35              # get size of largest cluster
36              max_size = max([i.area for i in rp])
37
38              # plug holes to make largest cluster even larger so it doesn't
get accidentally excluded
39              pixels['filled'] = ndimage.binary_fill_holes(pixels['closed2'])
40              # remove everything smaller than the largest cluster
41              pixels['cleaned'] =
morphology.remove_small_objects(pixels['filled'], min_size=max_size)
42
43
44              # plot the cropped, thresholded, and filtered images as subplots
45              #fig, ax = plt.subplots(1, 3, figsize=(8, 8), tight_layout=True)
46              #ax[0].imshow(pixels['labeled'])
47              #ax[1].imshow(pixels['filled'])
48              #ax[2].imshow(pixels['cleaned'])
49              #plt.title(filename)
50              #plt.show()
51              return pixels['cleaned']
52
53          if "SWE" in filename:
54              threshold = 100  # pixels with lower intensity than this value
are removed
55              colormap_threshold = 20  # pixel similarity tolerance
56              alpha = 0.5  # opacity of shear wave colormap overlay (default
50%)
57              offset = 667  # pixel separation between SWE and GS images
58
59              gsroibox = rawInput[288:824, 51:684]  # pixel box for GS half of
image
60              sweroibox = rawInput[288:824, 718:1351]  # pixel box for SWE
half of image
61
62              pixels['color'] = get_color_pixels(sweroibox, gsroibox,
threshold, colormap_threshold)
63              pixels['colormap'] = np.expand_dims(pixels['color'], axis=2) *
sweroibox
```

```python
64              pixels['composite'] = alphacomposite(sweroibox, gsroibox,
pixels['color'], alpha)
65              pixels['compositemap'] = np.expand_dims(pixels['color'], axis=2)
* pixels['composite']
66
67              # plot the cropped, thresholded, and filtered images as subplots
68              #fig, ax = plt.subplots(1, 3, figsize=(8, 8), tight_layout=True)
69              #ax[0].imshow(sweroibox)
70              #ax[1].imshow(pixels['colormap'])
71              #ax[2].imshow(pixels['compositemap'])
72              #plt.title(filename)
73              #plt.show()
74              return pixels['compositemap']
75
76
77     def get_color_pixels(sweroibox, gsroibox, threshold,
colormap_tolerance):
78          graybox = gsroibox.dot([0.07, 0.72, 0.21])  # convert RGB image to
grayscale
79          tendon_pixels = threshold_py(graybox, threshold)
80
81          # Check if the G and B values are close to R (R ≈ G ≈ B within
tolerance)
82          gray_pixels = np.all(np.isclose(sweroibox[:, :, :3], sweroibox[:, :,
0:1], atol=colormap_tolerance), axis=-1)
83          color_pixels = ~gray_pixels * tendon_pixels
84          cleaned_color_pixels = morphology.remove_small_objects(color_pixels,
min_size=500)
85          return cleaned_color_pixels
86
87
88     def alphacomposite(co, cb, color_pixels, a):
89          ca = np.clip((co - (cb * (1 - a))) / a, 0, 255)  # alpha compositing
90          result = ca.astype(np.uint8)
91          return result
```